Ligne InterFaces

I. INTRODUCTION

Un audit (Beamline Review Panel, BLRP) de la ligne CRG-Interfaces (IF) réalisé tous les cinq ans par un panel d'experts internationaux choisis par l'ESRF a eu lieu en mai 2010. Nous avons à cette occasion produit un rapport scientifique et technique couvrant les 5 dernières années. Le présent rapport est donc délibérément court, et ne vient que compléter le rapport pour l'audit. Les conclusions du panel d'expert sont reproduites ci-dessous.

En parallèle, le CEA/INAC a été évalué par l'AERES. L'évaluation de son laboratoire NRS portant essentiellement sur la ligne CRG-IF, nous en donnons aussi copie ci-dessous (seuls 2 scientifiques du CNRS/INéel et un ingénieur de recherche CNRS rattaché au CEA/SPram sont affectés sur la ligne sans être rattachés à NRS).

Cette année a vu la poursuite du développement de l'instrument de microdiffraction, grâce à l'acquisition de détecteurs bidimensionnels et de miroirs de microfocalisation à courbure fixe. Ce développement va se poursuivre grâce à l'obtention d'un nouveau projet ANR, dit AMOS.

L'objectif du projet P2N AMOS est de développer, comparer et standardiser les techniques de diffraction pour la mesure de l'orientation et de la déformation dans les nanodispositifs utilisés en microtechnologies et nouvelles technologies pour l 'énergie. Le projet vise à rassembler 3 techniques (Nanobeam Electron Diffraction (NBED), Convergent Beam Electron Diffraction (CBED) et microdiffraction X) autour des mêmes échantillons pour évaluer comparativement leurs atouts. Il vise aussi à développer des techniques d'analyse des données communes mettant en œuvre des principes et outils mathématiques similaires.

Cette année a aussi été mise à profit pour finaliser l'installation et la mise en fonctionnement de l'injection de gaz hydrures de semi-conducteurs sur l'instrument INS (*In situ* growth of Nanostructures on Surfaces, anciennement SUV). Nous avons profité d'un arrêt de l'installation lié à un incident sur la fenêtre de béryllium pour finaliser le montage, les tests et l'installation de la nouvelle tête porte-échantillon, que nous attendions depuis plusieurs années.

Les expériences de microdiffraction des dernières années produisent leurs premières publications à un bon rythme, comme l'atteste la liste en fin de rapport des articles publiés depuis le rapport d'audit. En parallèle les deux autres instruments continuent à alimenter des publications dans leurs domaines, dont certaines de grande qualité comme dans Europhysics Letters et Philosophical Magazine sur GMT et un article dans Nature issu de l'instrument INS.

Les deux évaluations mettent en avant la grande qualité des recherches conduites sur la ligne et son bon équipement, ainsi que deux recommandations concernant les moyens disponibles:
-remplacer l'ensemble diffractomètre + chambre ultravide de l'instrument *in situ* à moyen terme ;
-embaucher un scientifique sur la croissance *in situ* par CBE (UHV-CVD).

Le premier point met en avant l'obsolescence à moyen terme du cœur de l'appareillage d'étude de la croissance *in situ*. Si l'équipement ultravide, très conséquent, est tout à fait à jour, le diffractomètre lui-même montre des signes de faiblesse mécanique, et la chambre ultravide équipée d'une fenêtre de béryllium mériterait d'être remplacée par une chambre plus moderne, comportant notamment des fentes sous vide pour les mesures de GISAXS. Il s'agit donc d'un projet de jouvence important à envisager dans les années à venir.

Le second point relève la nécessité d'accompagner scientifiquement le développement technique réalisé ces dernières années sur l'installation INS permettant la croissance *in situ* en phase chimique (UHV-CVD ou CBE). La solution actuelle consiste en l'embauche d'un post-doc récurrent, qui assure en outre une partie du rôle de « local contact ».

En outre, si un technicien a pu être embauché en CDD au CEA pour un an, il serait très souhaitable de transformer son contrat en CDI, assurant ainsi la permanence du support technique.

Report of beamline review panel on BM32

General
The committee was impressed by the broad range and quality of the research, the staff and the instrumentation of beamline BM32. Several modifications have been made in the review period, and still the beamline has continued to produce many excellent papers. The committee congratulates the staff with these efforts.

BM32 is operated in a special way, because there is a strong team of senior scientists that is embedded in local institutions (CNRS and CEA in particular). Each of these scientists is formally connected to the beamline only for a limited fraction of his/her time. This mode of operation has allowed on the one hand a broad range of topics to be covered, but has on the other hand the danger that there is only limited coherence between the various topics. Gilles Renaud has been a strong leader of BM32 and, together with the other members, deserves praise for this crucial role. Renaud has become the undisputed leader in the field of (UHV) GISAXS and has several high-impact papers in this field.

In a CRG beamline in general, and BM32 in particular, it is difficult to separate the research from the users from that of the staff. In most cases, the research in the ESRF public beamtime still involves the people and laboratories of the beamline. Clear scientific highlights are the shape changes of Rh nanoparticles during oxidation and reduction (published in Science in 2008), the supercooling in AuSi eutectic droplets (published only weeks ago in Nature), the results on epitaxial InAs/InP nanowires (published in Nano Letters, 2007) and the interface structure after wafer bonding (e.g. Applied Physics Letters 2009).

Beamline instrumentation
Since the last review, two major improvements have been made. The first one is the beamline optics that was renewed in 2006. The committee was impressed by the excellent performance of the new optics, in which the flux is exactly what is theoretically calculated and in which the full 2 mrad acceptance of the front-end is used. The optics delivers a stable beam, with very little harmonics and the users are satisfied. The second improvement was the enlargement of the hutch with the UHV system. This major overhaul was done efficiently and has allowed new techniques and equipment to be combined with the existing set-up.

Microdiffraction
The involvement of staff in instrumental development is of the highest level. In addition, a stronger scientific interaction with beamline users is encouraged. The user community shows very promising results given the novelty of the technique, a further extension of the user base should be promoted.

The committee encourages the beamline scientists to further connect with other facilities and their users with the aim to contribute to establishing an international community. The committee strongly supports the further promotion of the aimed 3D-microdiffraction techniques in the material science community to establish excellence in scientific cases.

The committee is strongly impressed by the quality of the micro-diffraction instrumentation, specifically with regards to methods to determine the lattice parameter, 3D-strain microscopy and their contribution to analyzing software. Applications in 3D-Laue techniques will critically depend on improved acquisition speed which should be a high priority target of beamline development.

In situ nanostructures and surface (INS) station
Many achievements have been obtained using the joint facility of collecting in-situ data from GIXD and GISAXS, as an example the work on size and composition influence of CoPt nanoparticles morphology (PRL 100 (2008) 115502 . Outstanding results have been achieved on studies of substrate enhanced supercooling of eutectic droplets (Nature, 464 (2010) 1174). This topic will be developed in the future with the implementation of gas sources MBE. The whole series of experiments on Ge/Si(100) going from wetting layer to 3D growth include in-situ studies of state of the art surface diffraction, GISAXS and anomalous grazing incidence diffraction. Results on ultrathin metallic alloys are of interest for their magnetic properties. An in-situ control of these properties would be a plus.

E. Vlieg, J. Frenken, V. Holy, M. Sauvage-Simkin, R. Spolenak, H. Van Swygenhoven

The goniometer does not match the quality of the growth facilities and should be replaced.
The review panel acknowledges the effort in implementing the gas source MBE. Sufficient beamtime for commissioning the new equipment, which will be opened to users, should be provided. The MOKE project will enhance the quality of information on magnetic systems, it should be operated with minimal losses of beamtime use.

The number of topics currently pursued is very wide and seems to be more than the present staff can handle in the long run. We recommend concentrating on gas source MBE and magnetic systems and strengthening collaborations with expert groups in these fields. We recommend hiring one more person for running the gas source MBE to guarantee continuity of expertise.

Catalysis
The beamline is highly suitable for detailed investigations of model catalysts. An example of outstanding work in this field is the publication by Nolte *et al.* (Science **321** 1654, 2008) using the INS instrument. It is this type of detailed *operando* information that will lead to a full understanding of the structure and working mechanisms of 'real' catalysts.

The special setup constructed by Saint-Lager (CNRS, Grenoble) enables the investigation of model catalysts under the full pressure range, thus also beyond the pressure gap. The field of atomic- and molecular-scale catalysis research is rapidly moving away from flat surfaces to nanoparticles and from ultrahigh vacuum or low-pressure and low-temperature conditions to realistic reaction conditions.

The available diffraction techniques, dedicated instrumentation and expertise make BM32 extremely well-positioned to play a decisive role in these important and highly relevant developments. Therefore, the review panel suggests that the effort on catalysis at BM32 is strengthened, for example by actively searching further collaboration with expert groups in the field and, if possible, by providing access for other users also to Saint-Lager's setup.

Summary of recommendations
- Further promote interaction with leading groups in important scientific areas, in particular microdiffraction, gas source MBE and catalysis.
- Purchase new diffractometer for INS set-up.
- Develop fast data acquisition for 3D microdiffraction.
- Exploit fully the capabilities of new pixel detector for all techniques involved.
- Make sure the permanent staff is proportional to the number of topics pursued.
- Hire permanent scientist to do gas source MBE to ensure continuity of expertise.

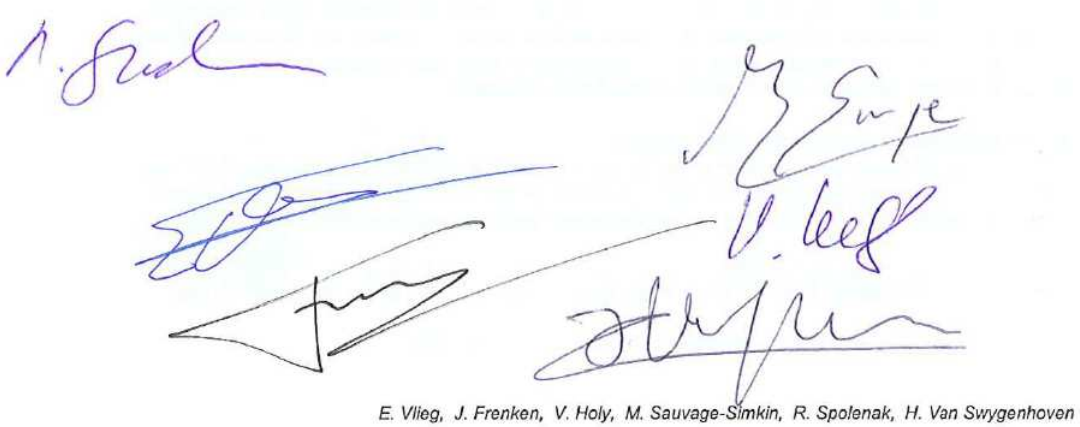

E. Vlieg, J. Frenken, V. Holy, M. Sauvage-Simkin, R. Spolenak, H. Van Swygenhoven

Extrait du rapport d'évaluation de l'AERES de l'INAC, relative au laboratoire NRS:

SP2M E12: X-Rays for Materials and Nanostructures

Scientific quality and production

In addition to its own research, the mission of the NRS team is to operate a CRG beamline devoted to surface scattering and white beam micro-diffraction at the ESRF to the benefit of the national and international community. The combination of advanced synchrotron tools with local fabrication facilities at INAC obviously opens wide possibilities and the team has developed original or even unique research axes using synchrotron radiation like the in-situ study of growth mechanisms of semiconductor nanostructures or wafer bonding.
On the more technical side, the methodological developments, like strain and interdiffusion measurements in nano-structures, and white beam micro-diffraction applied to stress/strain measurements are original.

Publications reported for the 2005-9 period are of a consistently high caliber. Of the ~75 major publications, there are 5 PRL 26 PRB, 8 APL and one paper in Science plus two patents and 17 invited talks. For a group of 9 full-time researchers, this represents an excellent output. A significant number of the papers, first-authored by external groups, originate from the operation of the CRG facility at ESRF. Based on comparisons with other facilities, there is about the correct ratio of internal selfmotivated projects to outside user experiments with contributing/helping authors within the group.

The NRS team participation to national projects is excellent and a significant number of international collaborations are reported (including a RTRA chair of excellence). The strong link to CEA-LETI and SOITEC (wafer bonding) is an excellent example of successful collaboration with industry.

International recognition and attractivity

The NRS Team is famous for its grazing incidence scattering studies of nanostructure growth mechanisms. The recent work on AuSi eutectic ordering and enhanced supercooling is for example an excellent example of the benefit of running a CRG beamline, as multiple periods of beamtime are necessary to examine a number of samples. It is also remarkable that this activity is well linked with INAC and SP2M priorities.

The SOITEC collaboration is a highly important opportunity that must not be allowed to escape from the group. SOITEC has the patents on the 'smartcut' technology that is likely to make it a very successful company, possibly supplying the raw materials of the whole electronics industry in the future. Building on the patent portfolio is the job of a seamless INAC (fundamental) - LETI (applied) - SOITEC interaction. Many questions need to be answered about the steps involved with smartcut, which are likely to lead to significant improvements in the technology as well as basic scientific insight.

The micro-diffraction facility is unique in Europe. It is a particularly good choice for a bending magnet at ESRF. The technique does not need undulator radiation, but it does benefit from a small source and high energy beams. The beamline has a very broad scope from mineralogy to catalysis and microelectronics.

Evaluation of the project

In the long term, the responsibility for running CRG beamlines might be considered as a liability, where INAC resources are 'wasted' on providing services to the user community at large. Instead, we recommend the view be taken that the CRGs are a big asset for the following reasons: i) “incidental” publications where the staff members are included in beamline user publications. ii) there is a strong element of leadership by control of the equipment. The optimization and exact configuration gives the home team a big advantage over outside users. The equipment can be used more effectively by those who build and maintain it.
There is a clear opportunity to pioneer techniques and take intellectual leadership of those. The micro white beam Laue diffraction is a good example which has no equivalent in Europe. A big local advantage will follow from developing the technique.

Conclusion

Strengths and opportunities

- High scientific quality of the team.
- First class synchrotron radiation beamline, with in particular a white beam micro-diffraction capability which is unique in Europe.
- Collaboration with LETI and SOITEC.

Weaknesses and threats

- There is a critical mass of personnel needed to run a facility like the CRG beamline. Everyone's productivity will suffer if they are short staffed and unable to handle the burden of outside users. This could happen as active team members have left or are going to retire.
- Some researchers in the group, possibly more involved in user support, are less active from the point of view of publications.

Recommendations

- Maintaining an appropriate level of staff should be considered as a high priority. Appropriate funding for future refurbishment should also be secured. It is not optimal that this is done at the SP2M level only.
- It is strongly recommended to develop internally a strong research program, consistent with other SP2M priorities using the micro-diffraction facility in order to bring the science done on this instrument at the level of excellence of the others. Collaborations with external groups about indexing software in order to identify multiple orientations simultaneously from a Laue pattern could also save time and efforts.
- The staff members who are publishing less should be encouraged to take the lead on scientific projects that are likely to lead to publication. They should be given the clear message that regular publication is important and possibly given mentoring by more established researchers.

II. DEVELOPPEMENTS INSTRUMENTAUX

II.1. Détecteurs

Dans ce domaine nous cherchons toujours à maintenir au meilleur niveau les ensembles de détection afin de proposer des instruments compétitifs et attractifs, utilisant au mieux les photons de notre aimant de courbure.

Nos travaux ont porté sur l'intégration dans notre système d'acquisition de 3 caméras et d'un détecteur pixel. Deux des caméras sont maintenant mises à disposition des expériences, la troisième est en phase finale de test ; le détecteur pixel a été utilisé pour la première fois sur GMT pour des tests et le logiciel doit encore être perfectionné.

On rappelle qu'en fin d'année précédente nous avions réceptionné 2 caméras pour la mircodiffraction, et une caméra pour les expériences de GISAXS sur INS ou GMT. Les développements logiciels faits pour cette dernière permettent de profiter pleinement de ses caractéristiques et notamment de son système d'antisaturation des pixels autorisant un signal de très forte intensité sans dégradation du signal dans les pixels voisins. Ceci est très appréciable pour les expériences de GISAXS pour lesquelles le signal utile peut se retrouver très prés du direct et être tout de même exploitable. Cette caméra est maintenant utilisée de manière routinière pour ce type d'expérience.

Le détecteur pixel (Fig 1a) a une surface de détection de 71.3x14.1 mm avec 1296 x 256 pixels, une efficacité de 68% à 15 keV (37% à 20 keV), un taux de comptage de 100 000 cps/pixel à 10% de temps mort, un temps de lecture de 3.5 ms, et un bruit de 1 coup/pixel/jour. Nous avons fait des tests de rocking scan sur un échantillon silicium-sur-isolant (SOI) obtenu par intégration en temps réel d'une ROI sur le détecteur. On voit (Fig 2) les deux pics correspondant au film de SOI (premier pic) et au substrat (second pic). Les oscillations à droite du pic de SOI correspondant à l'intersection de la tige de diffraction du film SOI avec la sphère d'Ewald.

Fig 1a : détecteur

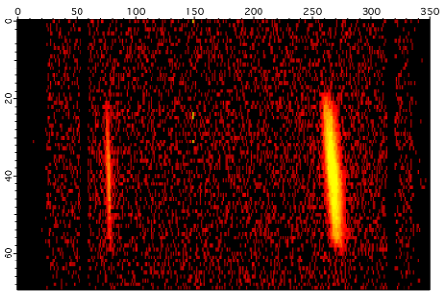

Fig1b : image d'un quadrant

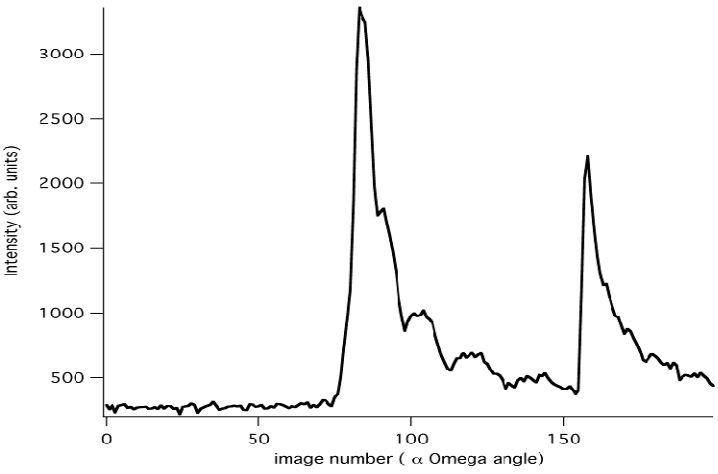

Fig 2 : Rocking scan obtenu en quelques minutes

II.2. Microdiffraction

Les deux caméras acquises pour la microdiffraction devaient répondre à deux exigences contradictoires, rapidité et sensibilité.

Les développements logiciels pour utiliser la caméra rapide VHR de Photonic Science (12bits, 2672x2672 pixels sur un champ circulaire de 81mm) sont terminés et celle-ci peut être utilisée pour les expériences dans lesquelles le signal est intense et le temps de pause supérieur à 1.5 seconde, typiquement pour les études de matériaux massifs. Dans ce cas, la lecture de la caméra se faisant durant l'exposition de l'image suivante, on a un temps mort qui est de quelques dizaines de ms, ce qui apporte un gain considérable lors de cartographies d'échantillons. Cette caméra étant globalement moins sensible d'un facteur 6, on compense donc par un temps d'exposition plus long mais au final, sur la durée totale de l'acquisition, on gagne encore un facteur 5 en temps.

La caméra Roper QuadRo 4096 (16 bits, 2048x2048 pixels sur un champ circulaire de 165 mm) sera opérationnelle en fin d'année. Nous travaillons actuellement aux dernières mises au point logicielles, pour intégrer les corrections lors des acquisitions. Cette caméra permet de capturer des images et de faire toutes les corrections en 2.6 secondes. Ceci représente un gain d'un facteur 2 par rapport à la caméra MAR 165 que nous continuons d'utiliser là où une bonne sensibilité est indispensable.

Les miroirs à courbure fixe permettant une augmentation de la densité de flux d'un facteur 10 par rapport aux miroirs ont été commandés chez JTEC au Japon. Ils seront livrés mi-novembre. Leur très faible erreur de pente (<0.2µrad) et leur rugosité inférieure à 2Å rms nous permettrons d'atteindre une taille de faisceau de 200x300µm. Notre choix pour la mécanique de support des miroirs s'est porté sur deux hexapodes permettant d'avoir dans un volume réduit tous les degrés de réglages indispensables au micro-positionnement des miroirs. Cet ensemble sera monté sur une table antivibratoire pour couper les perturbations mécaniques remontant par le sol. Ces ensembles sont financés dans le cadre d'une ANR AMOS (Nanotechnologie et Nanosystèmes).

II.3. Système d'injection de gaz pour les croissances en phase gazeuse dans INS

L'ajout sur l'installation INS du système d'injection de gaz a aussi demandé un travail important de la part du personnel de ligne et des post-doc, pour d'une part se conformer aux impératifs d'une utilisation en toutes sécurité des gaz dangereux tels le Silane et le Germane, et d'autre part pour intégrer ce système de dépôt au système de pilotage de l'instrument INS.

Pour être en conformité avec les règles de sécurité des personnes imposées par l'ESRF, et pour garantir le plus haut niveau de sécurité possible pour les utilisateurs futurs de cette installation, pour le personnel de la ligne, et pour les utilisateurs de BM32, nous avons en collaboration avec l'ESRF et la société VEGATEC développé le système de gestion des diverses alarmes. Ceci nous a conduits à définir les procédures d'intervention pour les maintenances, les modes opératoires en situation d'expérience, les procédures d'urgences, et les systèmes de mesure de gaz avec des redondances afin d'éviter les fausses alarmes.

Le pilotage de cette nouvelle installation se fait soit depuis la cabane d'expériences INS en utilisant un automate avec un écran tactile présentant un synoptique de l'installation et les divers points de mesures et consignes, soit depuis la salle de contrôle et la station de contrôle à l'aide d'un logiciel que nous avons développer et qui permet de gérer les cycles d'injection lors des expériences sous faisceau X.

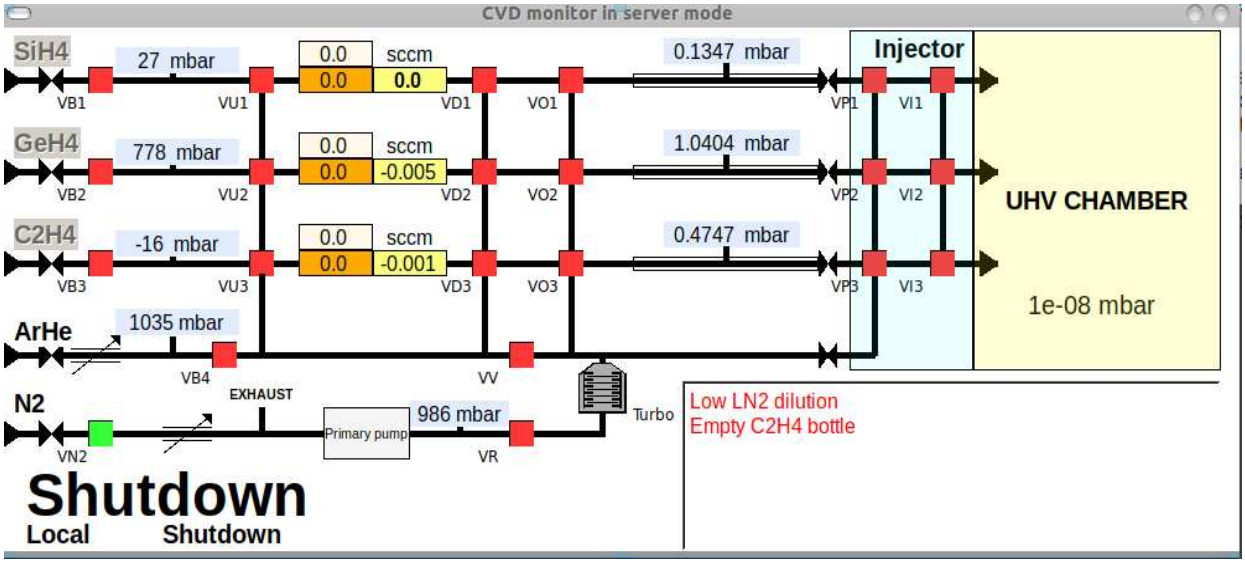

Fig 1 : Synoptique du système d'injection de gaz dans le logiciel de contrôle

II.4. Système informatique

Nous avons mis à niveau le système informatique de la ligne afin de suivre les évolutions du matériel et des systèmes d'exploitation. Nous nous appuyons maintenant uniquement sur des systèmes 64 bits avec des distributions Linux proposant des supports à long terme. Nous avons aussi étendue la capacité de stockage sécurisée en interne sur la ligne à 6 To (en plus des 2To de la station d'acquisition), afin de fournir un espace suffisant pour les données collectées par les détecteurs 2D.

III Goniomètre Multi-Techniques (GMT)

La cabane expérimentale a accueilli au cours de la période 2009-2010 des expériences utilisant le goniomètre multitechnique (diffraction et diffusion en faisceau monochromatique) et l'instrument de microfocalisation (diffraction combinée faisceau polychromatique-monochromatique). L'attrait pour ce dernier instrument se révèle par une majorité des demandes de temps de faisceau par la voie des comités international (ESRF) et français.

III.1. Goniomètre Multitechnique :

Les expériences conduites avec le goniomètre multitechnique couvrent les domaines traditionnels pour lesquels cet instrument est optimisé et permet des combinaisons entre techniques: réflectivité, diffraction rasante et cartographie d'espace réciproque utilisant des rayons X durs (30keV) pour étudier des interfaces ou objets enterrés (Rieutord *et al*), diffraction grands angles (diffraction de surface – mesures de contraintes) (St-Lager *et al*, Rieutord *et al*, Eymery *et al*, Letoublon *et al,* Biquard *et al*), diffusion aux petits angles en incidence rasante (St-Lager *et al*).

Une réflexion est menée pour optimiser l'utilisation des photons sur cet instrument afin de l'adapter aux nouvelles techniques de caractérisation combinant des détecteurs 2D et l'incidence rasante. Il s'agit aussi de faciliter son emploi (mesures et analyses) pour répondre à des demandes d'études systématiques en recherche appliquée. Des expériences préliminaires de faisabilité ont débuté pour cerner les besoins instrumentaux et logiciels. Nous nous sommes par exemple équipé d'un détecteur pixel de type Maxipix sur lequel des premiers essais ont été effectués (cf. site internet de la ligne rubrique goniomètre multitechnique: http://www.esrf.eu/UsersAndScience/Experiments/ CRG/BM32/Beamline/GMT/index_html).

III.2. Microdiffraction :

D'abord, cette année est marquée par l'arrivée des premières publications liées à l'emploi de l'instrument de microdiffraction. C'est le fruit d'un long travail technique de réduction drastique des vibrations et d'améliorations continuelles des procédures de réglage et d'acquisition. C'est aussi le résultat d'une analyse difficile et longue des données (en termes de complexité d'information et de volume de données). La communauté des utilisateurs a maintenant bien pris en main les outils d'analyses et est sensibilisée sur le mode opératoire de collection et de traitement des données (travaux pratiques microdiffraction à l'école du GDR Mecano, Autrans, Mars 2010).

Ensuite, le développement du code d'analyse des données LaueTools http://sourceforge.net/projects/lauetools/ a franchi une étape importante en permettant de réaliser toute la chaîne de traitement et d'analyse (recherche de pics, indexation, ajustement des paramètres de calibration du détecteur, ajustement de la déformation) en autonomie complète vis-à-vis du logiciel XMAS (développé à l'ALS, Berkeley, USA, http://xraysweb.lbl.gov/microdif/user_resources.htm). Les prochains jalons sont l'amélioration du traitement des diagrammes à plusieurs grains et l'analyse séquentielle (ou parallèle) d'un ensemble de diagramme récolté au cours d'une cartographie.

Enfin, nous avons réussi les premières expériences de microdiffraction résolue en profondeur dont l'objectif est de déterminer à trois dimensions l'orientation cristallographique locale et le déviateur des déformations élastiques. La méthode employée (Differential Aperture X-ray Microscope « DAXM » Larson et al Nature 415 (2002) 887) consiste à remonter au point d'émission des taches de diffraction en les masquant successivement à l'aide d'un fil se déplaçant au dessus de la surface de l'échantillon. Les premiers résultats sur un film d'UO2 implanté sont très encourageants.

Notons qu'il y a une demande forte pour la microdiffraction laue et en particulier pour la résolution 3D : en plus des deux lignes opérationnelles américaines 12.3.2 à l'ALS et 34-ID-E à l'APS. Les lignes VESPERS à CLS (canada) et B11 sur le synchrotron Australien ont été récemment

ouvertes et proposent de manière similaire (cartographie de fluorescence, microEXAFS et microdiffraction Laue). Un projet est à l'étude à Diamond (Angleterre) pour une ligne de métallurgie dédiée entre autre à la microdiffraction Laue.

L'ANR AMOS financera le positionnement mécanique des miroirs focalisant KB à courbure fixe, le filtrage actif des vibrations et l'acquisition d'un détecteur et carte électronique permettant de mesurer l'énergie de tâches de Laue et de remonter au tenseur complet des déformations. Dans ce cadre, l'automatisation de l'analyse des données en ligne sera développée.

III.3 Un fait scientifique marquant sur l'instrument GMT/Microdiffraction:

Philosophical Magazine
2010, 1–9, iFirst

Taylor & Francis
Taylor & Francis Group

Dislocation storage in single slip-oriented Cu micro-tensile samples: New insights via X-ray microdiffraction

C. Kirchlechner[ab]*, D. Kiener[ac], C. Motz[a], S. Labat[d], N. Vaxelaire[d], O. Perroud[d], J.-S. Micha[ef], O. Ulrich[ef], O. Thomas[d], G. Dehm[ab] and J. Keckes[b]

[a]*Erich Schmid Institute of Materials Science, Austrian Academy of Sciences, Austria;* [b]*Department of Materials Physics, Montanuniversität Leoben, Austria;* [c]*Materials Center Leoben Forschungs GmbH, Leoben, Austria;* [d]*IM2NP, Faculté des Sciences et Techniques de St Jérôme, Université Paul Cézanne, Marseille, France;* [e]*CEA-Grenoble, Institut Nanosciences et Cryogénie, Grenoble, France;* [f]*CRG-IF BM32, ESRF, Grenoble, France*

(*Received 20 November 2009; final version received 17 March 2010*)

Synchrotron X-ray microdiffraction was used to characterize the deformation structure of single crystalline Cu micro-tensile specimens which were oriented for single slip. The 3-μm thick samples were strained *in situ* in a scanning electron microscope (SEM). Electron microscopy observations revealed glide steps at the surface indicating single slip. While the slip steps at the surface must have formed by the predominant activation of the primary glide system, analysis of Laue peak streaking directions revealed that, even at low strains, dislocations had been activated and stored on an unpredicted slip system. Furthermore, the μLaue scans showed that multiple slip takes over at a later state of deformation.

Keywords: diffraction; dislocation structures; deformation mechanism; *in situ* electron microscopy; mechanical testing; plasticity

1. Introduction

It has been shown that the mechanical properties of single crystals become size-dependent in the micrometer and sub-micrometer regime, even when strain-gradient effects are minimized in uniaxial loading [1–7]. Regardless of experimental conditions and materials, an increase in strength with reduced sample dimension was usually observed. However, there is no thorough understanding of the underlying strengthening mechanisms, as can be seen from ongoing discussions on the two most prominent explanations for the size effects, namely truncation hardening [8] and starvation hardening [4]. In addition to *in situ* loading of the observation of sample deformation [5,7,9–12], there is also the need for a detailed structural investigation of deformation features.

Laue micro-diffraction (μLaue) is currently limited in lateral resolution to ~1 μm, but offers high angular resolution by probing the whole specimen volume and,

*Corresponding author. Email: christoph.kirchlechner@stud.unileoben.ac.at

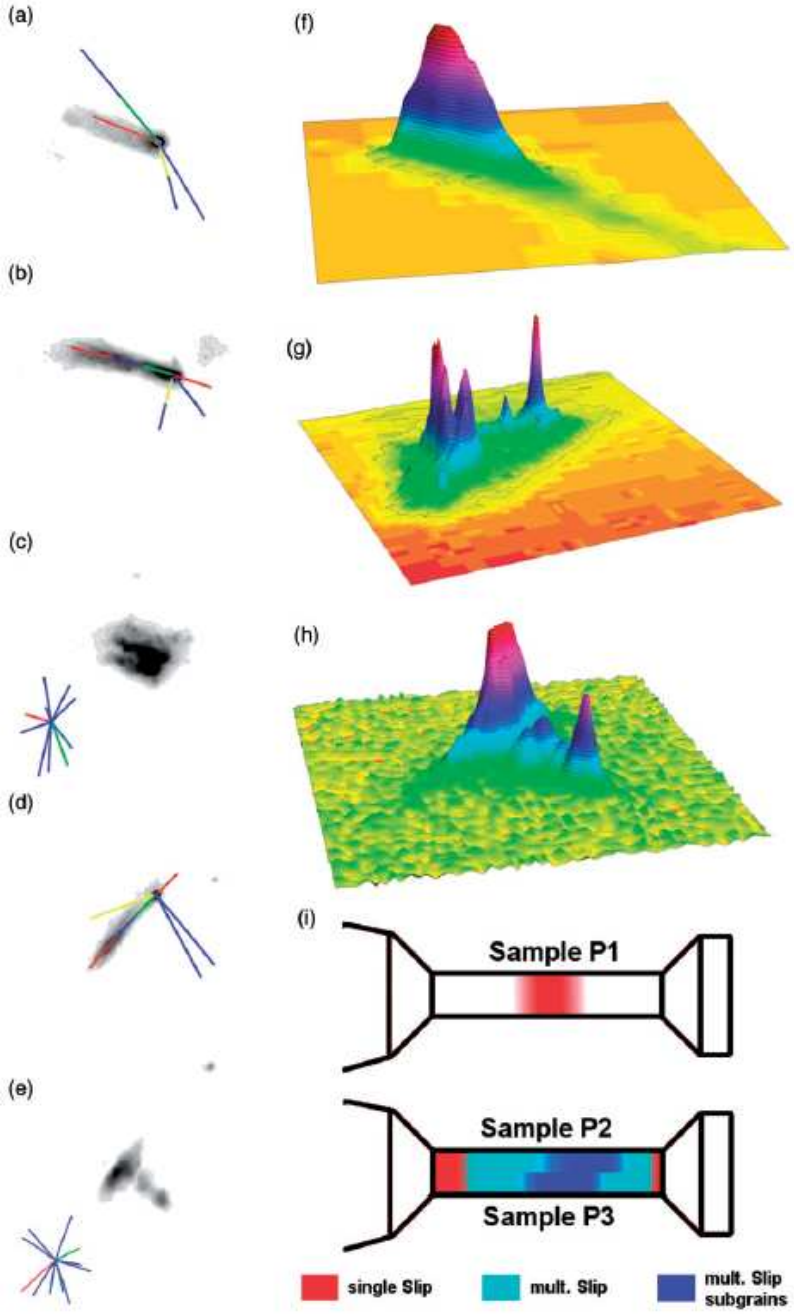

Figure 3. Representative Laue patterns: (a) $(6\bar{2}6)$ peak, P1 middle; (b) (111) peak, P2 near head and (c) in the middle; (d) (111) peak, P3 near head and (e) in the middle. The 3D peak profiles shown in (f)–(h) are the (111) peaks recorded in the middle of samples P1, P2 and P3. A slip-mechanism map, indicating if the diffraction data reveals single or multiple slip, is presented in (i).

Table 1. Schmid factors for all possible slip systems. For simplicity, an ideal ⟨234⟩ orientation is assumed for calculating the Schmid factors.

	Glide plane	Glide direction	Schmid factor
1	$(\bar{1}\bar{1}1)$	$[\bar{1}10]$	0.42
2	$(\bar{1}\bar{1}1)$	$[0\bar{1}1]$	0.35
3	$(\bar{1}\bar{1}1)$	$[\bar{1}01]$	0.30
4	$(\bar{1}11)$	$[\bar{1}10]$	0.25
5	$(\bar{1}\bar{1}1)$	$[01\bar{1}]$	0.21
6	$(\bar{1}11)$	$[01\bar{1}]$	0.13
7	$(\bar{1}11)$	$[\bar{1}01]$	0.13
8	(111)	$[\bar{1}01]$	0.10
9	$(1\bar{1}1)$	$[\bar{1}10]$	0.08
10	$(\bar{1}\bar{1}1)$	$[\bar{1}10]$	0.08
11	$(\bar{1}11)$	$[\bar{1}0\bar{1}]$	0.07
12	(111)	$[01\bar{1}]$	0.01

activated and caused the slip steps on the sample surface. This interpretation is supported by previous work of Ng and Ngan [20] on the activated slip system of micro-pillars and *in situ* μXRD studies on micro-compression samples [16]. Laue experiments are required to clarify this point for micro-tensile testing *in situ*.

In contrast, P2 and P3 (strained to 25%) showed different deformation features within the gauge length. In the region with the largest slip steps, multiple streaking directions and formation of sub-grains dominated the μLaue pattern. In most cases, it was not possible to identify all contributing slip systems. However, sub-grains were formed not only on the primary, but also on other systems, leading to a complicated peak shape as indicated in Figures 3g and h. Near the sample base and the head, contribution, other than the primary system, decreased, leading to an almost perfect single slip streaking direction caused by the storage of excess dislocations on the primary slip system. It is, therefore, concluded that multiple slip accompanied by the formation of subgrains dominated the deformation behavior in the middle of the sample, where the highest local strain (indicated by the large slip steps) was reached. Coincidentally, the gauge regions near the sample base and head still deformed in single slip on the primary slip system. This interpretation is in agreement with the local crystal orientations shown in Figure 2b.

4. Summary and conclusion

In situ SEM testing combined with postmortem μLaue diffraction experiments have been performed on single crystalline Cu micro-tensile samples. *In situ* SEM observations showed that only the predicted slip planes with the highest Schmid factor intersected the sample surface. μLaue experiments revealed that the sample base and head did not deform in any way. At low strains, dislocations of an unpredicted slip system caused peak streaking. They were not able to escape to the sample surface in larger numbers; thus, no similar slip steps were observed on the sample surface. At higher strains, multiple streaking directions were seen in the

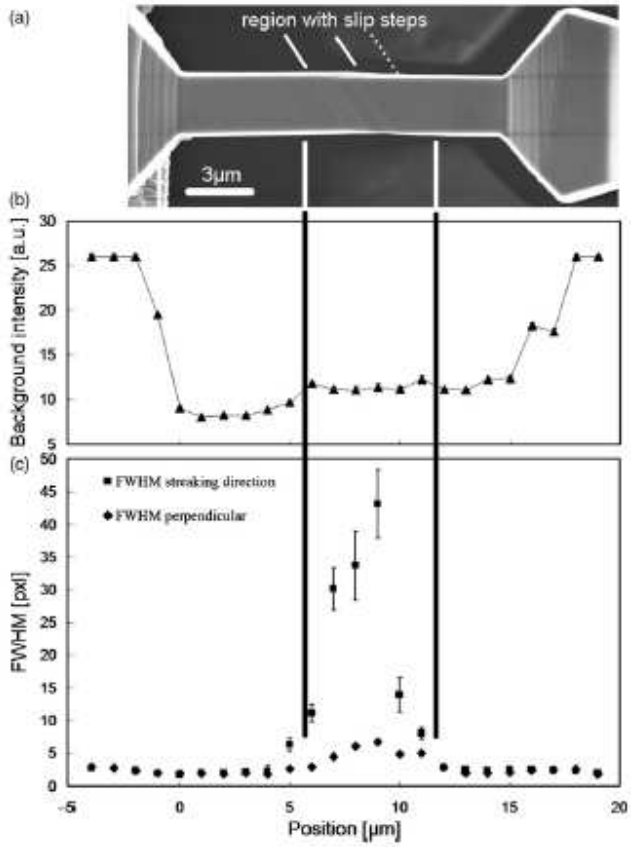

Figure 4. (a) SEM image of sample P1 (4% strain) with highlighted slip steps in the sample center. (b) Background intensity of the CCD was used for the correlation of the diffraction data with the SEM image. (c) Peak FWHM analysis of the (446) Laue spot: squares represent the FWHM in peak streaking direction, diamonds perpendicular to the streaking direction. The error bars are, in some cases, smaller than the plot markers.

center of the gauge length, accompanied by the formation of sub-grains. The near base and head regions still deformed in single slip on the primary slip system. *In situ* Laue experiments are capable of giving a greater insight into the deformation behavior of small-scale tensile samples.

Acknowledgement

A part of this work was supported by the Austrian NANO Initiative via a grant from the Austrian Science Fund FWF within the projects AP 26043-501 and P 17375-N07.

IV *In situ* growth of Nanostructures on Surfaces (INS)

IV.1. Introduction

Nous renvoyons au rapport au BLRP et aux conclusions du comité d'experts relativement à la qualité et à l'intérêt des mesures réalisées à l'aide de cet instrument (ayant notamment permis de réaliser une étude publiée dans Nature).

Rappelons que la cabane a été agrandies et rééquipée l'année dernière, et qu'un système de distribution de gaz réactifs y a été adjoint cette année. Nous avons aussi finalisé l'installation d'une nouvelle tête porte-échantillon plus précise et plus performante. Ces améliorations récentes multiplient les possibilités d'expériences et leur qualité, tout en améliorant grandement la sécurité des personnes et des biens.

De 2006 à 2009, l'équipe INS était composée de deux chercheurs CEA (T. Schülli et G. Renaud), d'un chercheur CNRS (M.de Santis) et d'un ingénieur de recherche CNRS (H. Tolentino). T. Schülli a été recruté par l'ESRF fin 2009 er remplacé par une postdoc, que nous souhaitons récurrent.

Depuis le départ de Marion Noblet-Ducruet, le support technique sur SUV a été insuffisant. Si l'aide très active d'Olivier Geaymond et l'embauche d'un jeune technicien sous forme de CDD d'un an ont permis en 2010 de réaliser le plus gros du travail technique, l'instrument SUV reste techniquement très complexe et demandant un suivi quotidien, nécessitant le travail d'au moins un technicien dédié, à plein temps. Il serait donc hautement souhaitable de stabiliser ce technicien sur un contrat CDI.

IV.2. Développements

La fenêtre de béryllium de la chambre ultravide intégrée au diffractomètre a été abimée mécaniquement, et a dû être renvoyée au Etats-Unis pour réparation. Du temps a été nécessaire pour définir et réaliser la solution technique adoptée (un collage avec une colle époxie spéciale) ; aussi l'instrument INS a-t-il été arrêté pendant six mois. Ce temps a été mis à profit pour réaliser plusieurs développements techniques (installation CBE, implémentation d'une nouvelle tête goniométrique porte-échantillon, d'un nouveau four et d'un support de la chambre) et pour tester l'injection de silane, à l'aide d'une chambre de dépannage. Nous décrivons brièvement ces développements ci-dessous.

IV.2.1. Mise en place d'une nouvelle tête goniométrique sur la chambre UHV.

Le remplacement de la tête goniométrique était urgent au vu des problèmes de reproductibilité de l'ancienne. Diverses améliorations ont été apportées lors de cette jouvence : améliorations techniques en termes de répétabilité et de précision des mouvements, ajouts de nouveaux mouvements dans le même encombrement, évolution complète du four porte échantillon tenant compte de l'expérience acquise avec les précédents modèles.

Améliorations mécaniques :

- pour faciliter l'étude de surfaces nanostructurée (nano fils, boites quantiques, surface fonctionnalisée par faisceau d'ion FIB) deux directions de déplacement de l'échantillon ont été ajoutées dans le plan du faisceau. La tête se déplace maintenant dans les trois directions de l'espace : z pour introduire l'échantillon dans le faisceau, x et y pour le déplacer parallèlement aux rayons X ;
- deux mouvements en berceau permettent d'aligner le plan de l'échantillon avec l'axe du faisceau et de conserver cette planéité lors de rotation de l'échantillon. La majorité des études

étant effectuées proche de l'angle critique des échantillons, une variation de l'angle d'incidence de l'ordre du centième de degré lors de la rotation de l'échantillon entraînerait une perte de signal de la surface. Une attention particulière à été apportée à la précision et au découplage de ces deux mouvements ;
- diverses mesures (comparateur) et expériences (rayon X) ont montré une reproductibilité parfaite des mouvements : z et les deux berceaux (χ_1 et (χ_2).

Le porte échantillon chauffant a été complètement repensé :
- pour éviter l'usure due à l'exposition des parties mécaniques à de très haute températures (ressort, parties vissées) une amenée d'eau permet de refroidir la partie arrière du four et sert par la même occasion de ressort pour le maintient de l'échantillon ;
- divers écrans permettent : dans la partie UHV d'éviter un dépôt de matière sur les céramiques (par exemple des métaux la rendant conductrice) en même temps qu'il atténue le rayonnement du four, dans la partie mécanique de la tête un écran à circulation d'eau permet d'éviter d'exposer les moteurs de la tête à de très hautes température lors de l'étuvage de la chambre UHV ;
- des développements en cours permettront de compléter ces efforts pour gagner en vide lors d'utilisation du four à très haute température (jusqu'à 1300° C).

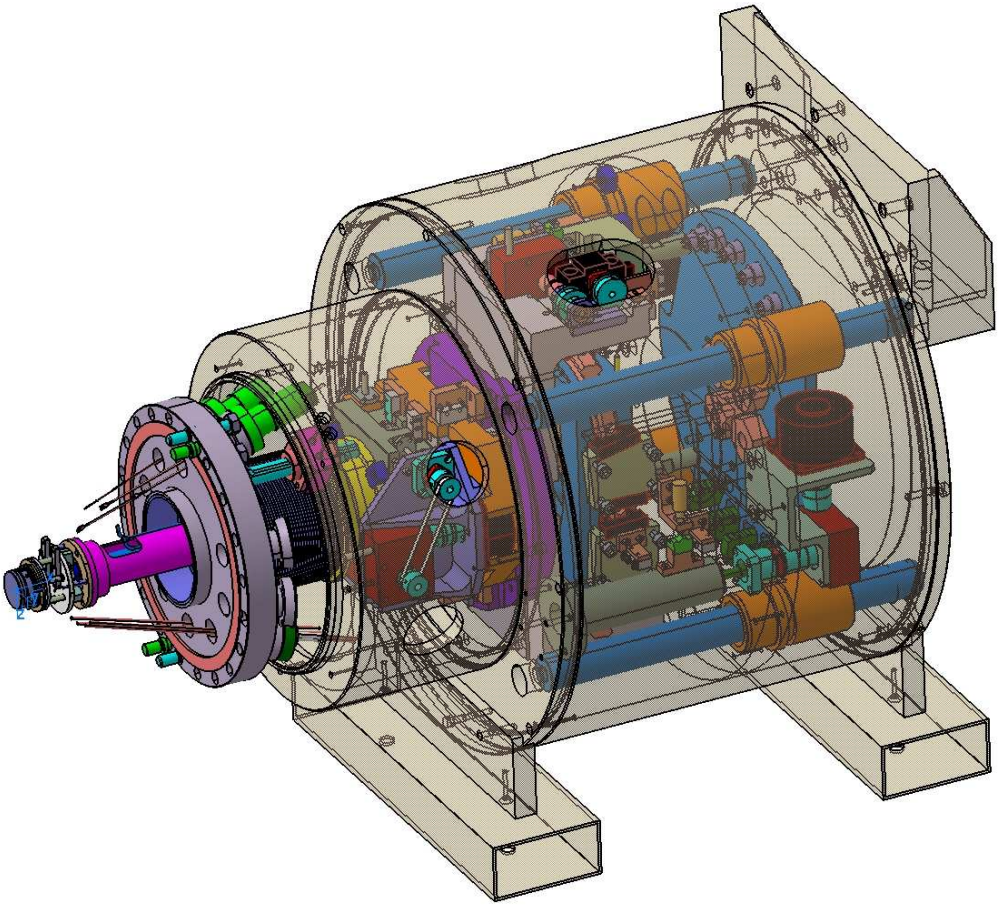

Schéma de la nouvelle tête porte-échantillon de l'instrument INS.

VI.2.2. Mise en place d'un système d'injection de gaz compatible silane (SiH_4), germane (GeH_4) et éthylène (C_2H_4) et premières expériences.

Dans la communauté scientifique internationale l'intérêt pour le nanofils de semi-conducteurs a fortement augmenté dans les dernières années et est justifié par les nombreuses applications technologiques comme la photovoltaique et les bio-sensors.

La façon la plus étudiée de faire des nanofils utilise la croissance dite Vapeur-Liquide-Solide (VLS) [1]. Un catalyseur métallique (Or ici) est déposé sur un substrat de Si ou Ge à la température ambiante, le traitement thermique suivant favorise la constitution d'ilots que sont ensuite fondus à basse température par la formation d'un eutectique par la diffusion du Si ou Ge dans le cluster d'Or (T_{eu} = 363℃, avec 19 atome % de Si; T_{eu} = 350℃, avec 27 atome % de Ge [2]). Un flux de gaz précurseur (SiH4 ou GeH4) est donc injecté dans la chambre de déposition à la température du substrat entre 350-700℃, la molécule d'hydrure se brise au contact de la surface du catalyseur en augmentant la concentration de Si ou Ge dans l'ilot métallique. Une fois la super-saturation obtenue, il y a nucléation des semi-conducteurs à l'interface entre l'ilot et le substrat en causant la croissance du nanofil au-dessous du catalyseur.

Les mécanismes physiques et chimiques qui gouvernent la croissance des nanofils ne sont pas encore complètement compris. Les modèles théoriques élaborés pour la description du processus de croissance par Déposition Chimique en phase Vapeur (CVD) sont fondés sur des résultats après des études en microscopie électronique effectués après croissance en exposant l'échantillon à l'air et à la température ambiance. Les conditions d'observation des nanofils sont donc très différentes des conditions de leur formation. De plus, les propriétés physiques et électroniques des nanofils sont strictement liées à leurs caractéristiques cristallographiques. Avec le système de CVD installé sur l'instrument INS, on se propose d'étudier les conditions de la nucléation et de la croissance organisée de nanofils de Si et Ge sur des substrats de silicium, et d'en étudier la structure, l'organisation et la morphologie au-cours de la croissance *in situ*, en utilisant le rayonnement synchrotron.

Le système d'injection de gaz, installé par la société Vegatec, peut contenir trois bouteilles de gaz inflammables, explosifs et/ou toxiques, tels que le silane, le germane et l'éthylène.

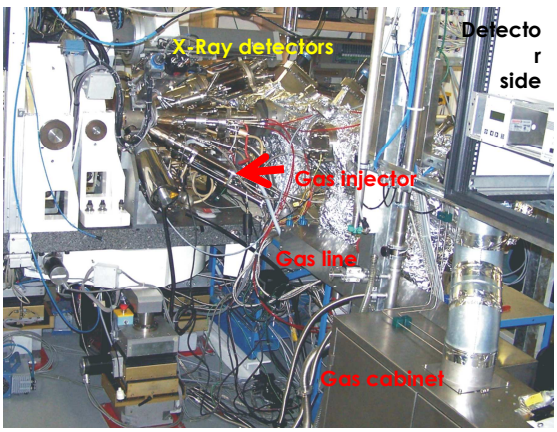

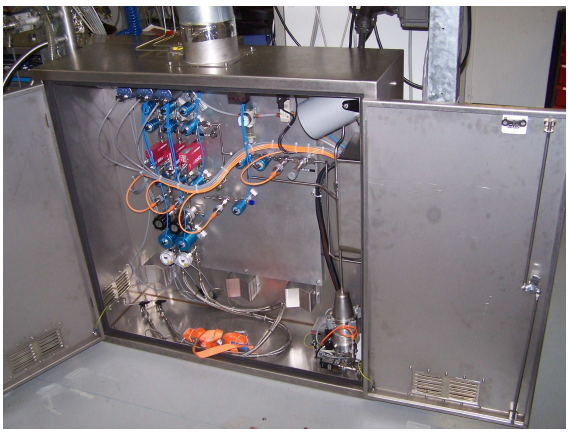

Photo 1 et 2: Photographie de l'armoire à gaz et de l'ensemble de l'instrument

Il consiste en une armoire ventilée en permanence (voir photos 1 et 2), et connectée à une cheminée d'extraction spéciale, munie de détecteurs de gaz et de feu, d'extraction, de pressions et de débits, et dont toutes les vannes, régulateurs de pression et de débit sont automatiques (voir figure et schéma). L'ensemble est géré par une électronique intégrée, programmée pour réaliser les différentes opérations telles que purges ou dépôts de façon automatique et en prenant compte tous les cas possibles de défauts de sécurité. Une interface utilisateur intégrée au programme de pilotage des instruments a été réalisée localement. Un document très complet de sécurité a été écrit, et les personnels ont suivi les différentes formations requises.

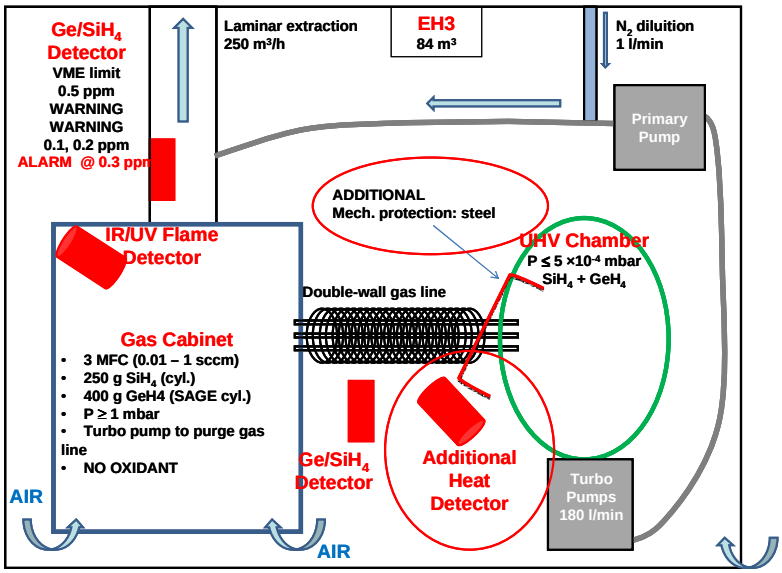

Schéma de l'ensemble de distribution de gaz.

L'injecteur de gaz est intégré à la chambre ultravide (voir schéma). Il permet donc de conserver les excellentes conditions de vide ($2x10^{-11}$ mbar) de la chambre pour toutes les expériences de déposition par évaporation physique de matériaux (MBE), tout en permettant l'injection de gaz ultra-purs entre 10^{-8} mbar et $5x10^{-4}$ mbar, à l'aide de vannes rapides, permettant de contrôler précisément les dépôts par voir gazeuse correspondants. L'injection à basse pression provoque un jet moléculaire qui est bien orienté par un cône de guidage à l'intérieur de la chambre UHV, générant une pression locale plus élevée sur la surface de l'échantillon.

Quinze jours de faisceau ont été dédiés aux premiers essais, révélant un fonctionnement entièrement conforme à nos attentes, hormis une pression résiduelle de méthane, 40 fois plus faible que celle de silane, induite par une réaction du silane avec tous les métaux chauds et comprenant du carbone autour de l'échantillon (en particulier les pièces du four). Ce problème devrait être résolu à l'avenir en focalisant le faisceau gazeux au centre de l'échantillon à l'aide d'un capillaire en quartz.

Schéma de la chambre UHV avec son injecteur de gaz.

- Gases: SiH_4, GeH_4, C_2H_4
- Max working pressure = 5 x 10^{-4} mbar
- Completely automatic gas injection system according to the ESRF security standards

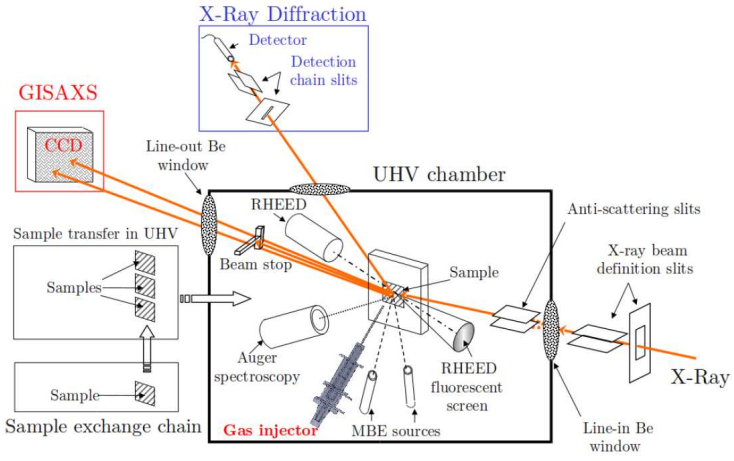

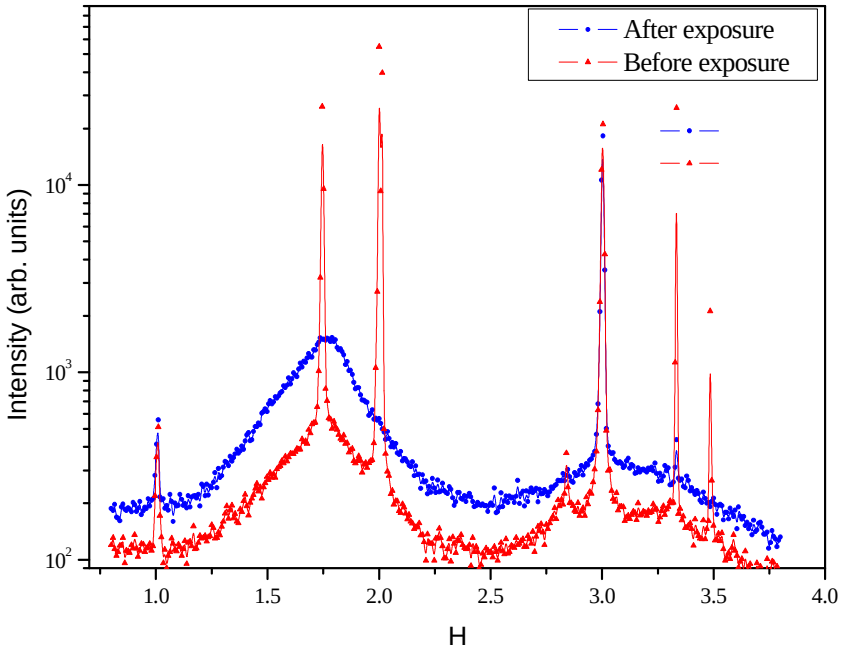

Mesure en incidence rasante parallèle à la surface de l'échantillon avant et après exposition au SiH_4 (0.9 sccm, 9 x 10^{-5} mbar).

Dans la première semaine d'expérience synchrotron, on a effectué des études *in situ* des dépôts d'Or sur un substrat de Saphir et suivi leur l'évolution durant l'exposition à différents flux de SiH_4 à diffèrent températures. La figure ci-dessus montre la transformation d'îlots d'Au cristallins (pics de Bragg) en gouttes liquides d'alliage (AuSi) par exposition au SiH_4 à température constante du fait du craquage de la molécule de SiH_4 à la surface des îlots.

A cause du débit très faible de gaz précurseur, la nucléation du Si en-dessous des gouttes d'or n'a pas encore été observée. Pour cette raison une amélioration du système est déjà prévue pour le début de 2011 avec un capillaire en quartz pour mieux guider le gaz sur la surface du dépôt, augmentant la pression locale mais préservant la pression totale de la chambre pour éviter de contaminer les autres équipements installés dans la chambre de croissance.

[1] R. S. Wagner, W. C. Ellis, Appl. Phys. Lett. 4, (1964) 89
[2] http://www.crct.polymtl.ca/fact/documentation/SGTE/SGTE_Figs.htm
[3] T. U. Schülli, R. Daudin, G. Renaud, A. Vaysset, O. Geaymond, A. Pasturel, Nature 464, 1174 (2010).

IV.2. Un fait scientifique marquant sur l'instrument INS:

L'étude de la surfusion dans des gouttelettes d'or sur substrats de Si(111), que nous avons brièvement évoqué l'an dernier a été publié dans la revue Nature. Rappelons que ces goutelettes sont des catalyseurs précurseurs de la croissance de nanofils.

Nous reproduisons ci-dessous l'article ainsi que le « News and Views » correspondants.

nature Vol 464 | 22 April 2010 | doi:10.1038/nature08986

LETTERS

Substrate-enhanced supercooling in AuSi eutectic droplets

T. U. Schülli[1,2], R. Daudin[1], G. Renaud[1], A. Vaysset[1], O. Geaymond[3] & A. Pasturel[4]

The phenomenon of supercooling in metals—that is, the preservation of a disordered, fluid phase in a metastable state well below the melting point[1]—has led to speculation that local atomic structure configurations of dense, symmetric, but non-periodic packing act as the main barrier for crystal nucleation[2,3]. For liquids in contact with solids, crystalline surfaces induce layering of the adjacent atoms in the liquid[4,5] and may prevent or lower supercooling[6]. This seed effect is supposed to depend on the local lateral order adopted in the last atomic layers of the liquid in contact with the crystal. Although it has been suggested that there might be a direct coupling between surface-induced lateral order and supercooling[6], no experimental observation of such lateral ordering at interfaces is available[6]. Here we report supercooling in gold-silicon (AuSi) eutectic droplets, enhanced by a Au-induced (6 × 6) reconstruction of the Si(111) substrate. *In situ* X-ray scattering and *ab initio* molecular dynamics reveal that pentagonal atomic arrangements of Au atoms at this interface favour a lateral-ordering stabilization process of the liquid phase. This interface-enhanced stabilization of the liquid state shows the importance of the solid–liquid interaction for the structure of the adjacent liquid layers. Such processes are important for present and future technologies, as fluidity and crystallization play a key part in soldering and casting, as well as in processing and controlling chemical reactions for microfluidic devices or during the vapour–liquid–solid growth of semiconductor nanowires.

Clusters with icosahedral short-range order are now widely considered as basic structural elements of liquid metals and glasses[3,7–9]. Their presence has been proven experimentally[4,7,10] and by *ab initio* molecular dynamics simulations (MDS)[11]. At solid–liquid interfaces, however, a description of the structure of liquids is difficult, as is the prediction of the influence of interfaces on ordering and more particularly supercooling. As highlighted in ref. 6, the degree to which a liquid can be supercooled strongly depends on the substrate in contact with it, as well as on thermal history. In recent experiments, enhanced layering in liquids at solid (crystalline)–liquid interfaces has been observed[4,5]. However, tracking its influence on crystallization or supercooling requires an investigation of ordering in the liquid along the interface, which presents an experimental challenge. In the present work, we analyse the influence of different interfaces on the degree of supercooling and possible in-plane order in AuSi liquid droplets of near-eutectic composition. The effects of three substrates—Si(001), Si(111) with a Au-induced $(\sqrt{3}\times\sqrt{3})R30^\circ$ reconstruction, and Si(111) with a Au-induced (6 × 6) reconstruction—are compared. Offering fluidity at low temperatures, such eutectic liquids are at the heart of the catalytic growth of semiconductor nanowires by the vapour–liquid–solid process[12]. Recent *in situ* microscopy studies of the growth dynamics and nucleation of semiconductor nanowires[13–15] suggest that Ge nanowires can grow below the AuGe eutectic temperature[16,17], with the catalysts' state depending on thermal history. Furthermore, a possible modification of the eutectic temperature for nanostructures has been suggested[18]. These puzzling observations call for further investigations of the supercooling behaviour of metal-semiconductor alloys and their atomic structure at semiconductor interfaces.

We used *in situ* grazing incidence X-ray scattering in ultrahigh vacuum at beamline BM32 of the European Synchrotron Radiation Facility to study solid–liquid transitions on surfaces and nanostructures[4,19]. The experimental results were compared to *ab initio* MDS[11]. The experiment consisted in analysing, for different temperatures, the atomic structure of the silicon surface, that of the liquid/solid Au(Si) islands, and that of the AuSi/Si(111) (or AuSi/Si(001)) interface, special attention being paid to a potential correlation between them. The different steps of the experiment are schematically shown in Fig. 1. The complexity of this system required mapping extended regions in reciprocal space (Fig. 2a), to address all structural features at a given temperature. These extended reciprocal space maps were performed by variation of the momentum transfer $Q = 4\pi \sin(\theta)/\lambda$, where λ is the X-ray wavelength and θ half the scattering angle between the incident and scattered beams that are almost parallel to the sample surface (for details on experimental tools and sample preparation, see Methods Summary, Supplementary Information, and Supplementary Figs 2 and 4).

During annealing (Fig. 1, steps 2–3), the Au islands transform into liquid droplets exactly at the bulk eutectic temperature, $T_E = 636 \pm 5$ K, suggesting that the Si substrate provided atoms to reach the $Au_{81}Si_{19}$ eutectic composition. All diffraction peaks from Au disappear simultaneously at T_E and give way to a scattering signal that is characteristic of a liquid phase, as shown on the reciprocal space map of Fig. 2a. For annealing temperatures higher than $T_E + 40$ K (=676 K) and subsequent cooling (Fig. 1, step 4) more diffraction peaks appear, corresponding to a well defined Si(111)-(6 × 6) superstructure[20], as revealed in the reciprocal space map in Fig. 2a. When cooling down below T_E, no Bragg peaks from solid Au reappear, but the liquid-like scattering remains: the islands stay liquid. Cooling down further reveals that solidification happens only at $T_S = 513 \pm 5$ K (Fig. 1, step 5), that is, more than 120 K below T_E. After solidification, the (6 × 6) superstructure remains, together with powder diffraction rings from the face-centred-cubic (f.c.c.) Au structure. Reciprocal space maps for different sample preparations are shown in Supplementary Fig. 4.

Remarkably, this phase transition is found to be fully reproducible: when the temperature is cycled down and up, the above-described behaviour of the solid–liquid–solid transition remains: melting at T_E on heating, and solidification at $T_S = 513 \pm 5$ K on cooling. Moreover, the final T_S value is independent of the time spent (between a few tens of minutes to a few tens of hours) at T_S or between T_S and T_E. Several samples were investigated with the procedure described above, or with co-deposition of an $Au_{81}Si_{19}$ film with the eutectic composition, all

[1]CEA, Institut Nanosciences et Cryogénie, SP2M, 17 rue des Martyrs, 38054 Grenoble, France. [2]European Synchrotron Radiation Facility, BP 220, 38043 Grenoble, France. [3]Institut Néel, CNRS, BP 166, 38042 Grenoble, France. [4]SIMAP INPG, BP 75, 38402 Saint Martin d'Hères cedex, France.

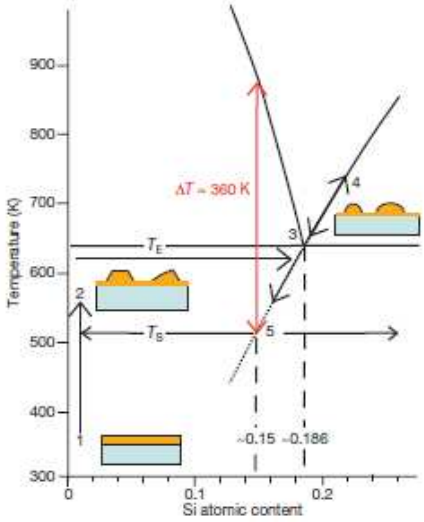

Figure 1 | Extract from the bulk AuSi phase diagram together with representations of the melting and solidification cycles of AuSi islands on an Si(111)-(6 × 6) reconstructed surface. The numbers 1 to 5 refer to successive experimental steps, and the large black arrows indicate the pathways followed by the islands during heating/cooling cycles. Seven monolayers of Au are deposited at room temperature (step 1; bottom inset). On annealing they transform into crystalline Au islands (step 2; middle inset). At $T_E = 636$ K, melting sets in and AuSi droplets with the eutectic composition ($Au_{81.4}Si_{18.6}$) are formed (step 3; top right inset). Heating up to 673 K before cooling (step 4) induces a (6 × 6) reconstruction, and leads to a preservation of the liquid phase down to 513 K (step 5), where phase separation and solidification occur (step 5). Above T_E, on heating or cooling, the liquid composition is expected to follow the Si liquidus. Below T_E, it follows the (extrapolated; dotted line) metastable Si liquidus. The degree of supercooling (red arrow) has to be measured between this latter and the Au liquidus above T_E for the corresponding composition of ~15 at.% Si. It amounts to ~360 K.

showing the same solidification temperature after cyclic melting and solidification.

The structure factor $S(Q)$ of the liquid in its supercooled state is shown in Fig. 3a. Very close to the origin (Fig. 3b), powder diffraction peaks are present, located exactly at the positions expected for the two-dimensional Au-Si crystalline structures reported to form on the surface of the liquid eutectic[21]. Figure 3e shows the intensity evolution around the first maximum of $S(Q)$ for decreasing temperatures through $T_S = 513$ K. The initially very broad intensity distribution narrows progressively approaching the solidification temperature, below which it collapses to give rise to the Au(111) Bragg peak. Hysteresis loops extracted from the integrated intensity of Au Bragg reflections (Supplementary Fig. 2) are shown in Fig. 3c for different Si surfaces and/or surface preparation. The lowest solidification temperature $T_S = 513 \pm 5$ K is observed for droplets on an Si(111)-(6 × 6) surface reconstruction, whereas it is significantly higher ($T_S = 563 \pm 5$ K) when heating the sample just above T_E, which only yields a precursory $(\sqrt{3} \times \sqrt{3})R30°$ reconstruction (Supplementary Fig. 4c). Proceeding similarly on an Si(001) surface (on which no reconstruction coexists with the liquid) only yields $T_S = 573 \pm 5$ K (Supplementary Fig. 3b). In all cases, peaks of the two-dimensional AuSi surface crystallites (Fig. 3b) were present and the deposited amount of Au was identical, leading to droplet sizes of 150–200 nm, too large to influence the solidification temperature. Remarkably, the size dependence is found to be weak for deposits between two and seven monolayers of Au ($T_S = (510–520) \pm 5$ K). One sample with a 30-monolayer Au deposit was investigated, yielding $T_S = 555 \pm 10$ K (Supplementary Fig. 7). This last value approaches that of $T_S = 573 \pm 5$ K, obtained when the Si

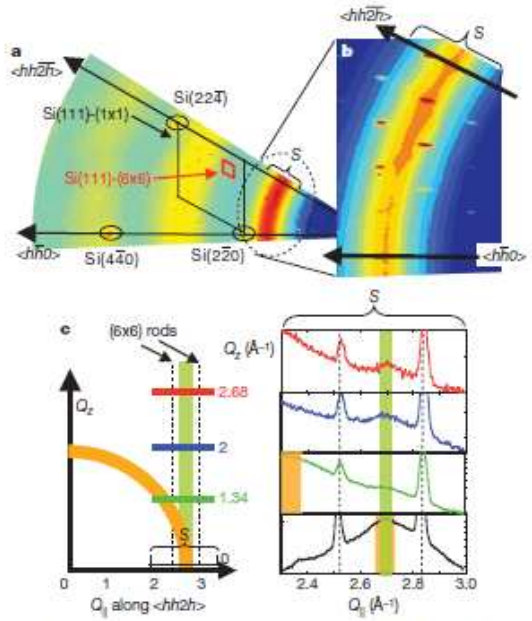

Figure 2 | Reciprocal space mapping of liquid AuSi islands on (6 × 6) reconstructed Si(111). a, Reciprocal space map of the liquid in its supercooled state on a (6 × 6) reconstructed Si(111) surface. Blue colour corresponds to low intensity, and red to high intensity, yellow being intermediate. Three bulk Bragg peaks are visible, together with a mesh of smaller peaks arising from the (6 × 6) surface/interface periodic superstructure. The three diffuse rings correspond to liquid-like scattering. **b**, Anisotropy of the first order maximum of the liquid structure factor: In the vicinity of strong (6 × 6) reconstruction peaks the signal from the liquid is enhanced, underlining morphological similarities between the crystalline surface and the adjacent liquid layers. **c**, Right: scans across the first order maximum of the liquid structure factor in the plane (along section S marked in **a** and **b**) and parallel to it for several values of out-of-plane momentum transfer, Q_z. Left: the sketch indicates in orange the position of the first maximum of the isotropic liquid. The green rod corresponds to the intensity distribution stemming from preferential in-plane order.

surfaces suffered from non-ideal preparation conditions (for example, carbon pollution), and is similar to values observed in a closed AuSi system without Si reservoir[22].

The decrease of the solidification temperature T_S when the surface is reconstructed (that is, the Si(111)-(6 × 6)Au reconstruction) and with increasing interface/volume ratio shows the crucial role of this particular interface structure on the conservation of the liquid state. This suggests that the specific local atomic structure at the interface favours peculiar ordering effects in the adjacent liquid layers, eventually lowering the interface energy and rendering it a particularly inefficient nucleant for Au. Other crystallization mechanisms may be dominant, such as faceting of the free surface[23] or homogeneous nucleation of Au triggered by concentration fluctuations. The composition of the supercooled droplets may favour the latter process; Si regrowth through a (6 × 6) reconstruction is possible without perturbing this surface structure (Supplementary Fig. 8). This demonstrates that this reconstruction does not inhibit the redeposition of Si at the interface below the droplet while it adapts its composition to follow the Si liquidus line when cooling from above T_E, reaching the eutectic composition at T_E. Below T_E, the droplet's composition is expected to follow the metastable Si liquidus (Fig. 1, step 5). At 513 K, the liquid being Au enriched by ~3–4 at.% with respect to the eutectic composition (Fig. 1), the corresponding degree of supercooling has to be measured between the Au liquidus of the equilibrium phase diagram above T_E and the metastable (extrapolated) Si

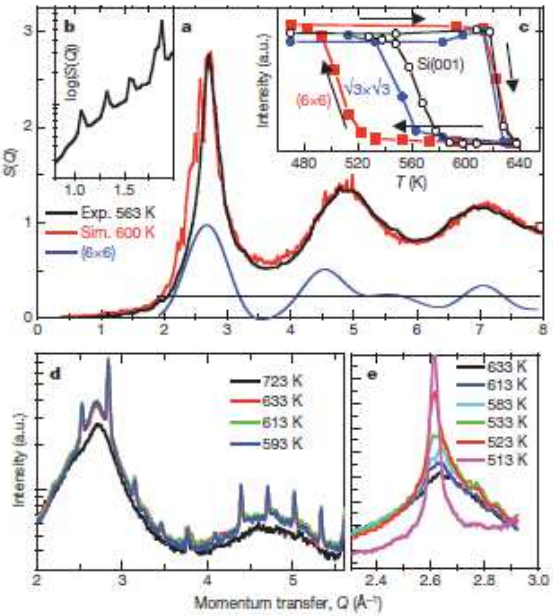

Figure 3 | Evolution of the liquid structure factor during cooling and solidification. **a**, Angular average of the experimental structure factor $S(Q)$ of liquid AuSi at 563 K (black line) together with the theoretical structure factor extracted from MDS at 600 K (red line). The blue line corresponds to the mean structure factor of the (6×6) reconstruction (Supplementary Fig. 5). **b**, Zoom (logarithmic scale) on the low-Q spectrum of the structure factor, showing the Bragg peaks from two-dimensional crystallites floating on the surface of liquid AuSi (ref. 21). **c**, Hysteresis loops of the integrated intensity of the Au(220) Bragg peak during the solid–liquid–solid transition of Au islands on Si(001) (black open circles), on an Si(111)-$(\sqrt{3}\times\sqrt{3})$R30° reconstruction (blue filled circles) and on an Si(111)-(6×6) reconstruction (red squares). **d**, Liquid structure factor (logarithmic scale) along the $<1\bar{1}0>$ crystallographic direction of the Si(111) surface. The strong influence of the appearance of the (6×6) reconstruction on the structure of the liquid is visible. **e**, Evolution of the first maximum of the liquid structure factor in the supercooling regime.

liquidus below T_E (red arrow in Fig. 1); this yields a remarkably large value of ~360 K.

Our experimental observation is further supported by *ab initio* MDS (see Supplementary Information for details) that allowed monitoring the structural evolution at three temperatures, above and below T_E. The $Au_{81}Si_{19}$ system was considered to be the prototype liquid for near-eutectic compositions; a change of 3–4 at.% Si does not modify the conclusions drawn from the structural analysis. The alloy was found to stay liquid even at 500 K, that is, well below T_E (Supplementary Fig. 9). The simulated liquid structure factor $S(Q)$ compares very well with the experimental one (Fig. 3a), confirming the accuracy of the simulations. To learn more about the detailed three-dimensional picture of the local structure of the liquid, we performed a common-neighbour analysis[24], which allows us to distinguish between various local structures, such as f.c.c., hexagonal close packed, body centred cubic, and icosahedral environments. The short-range order is found to display an appreciable proportion (46%) of pairs in local five-fold arrangement in the liquid state ($T = 700$ K); the supercooled regime is characterized by an increased fraction of five-fold atomic ordering (51% at $T = 600$ K and 54% at $T = 500$ K). The temperature dependent occurrence of five-fold clusters is shown in Supplementary Fig. 10.

Solid–liquid systems that present important interface-induced atomic layering (that is, short range order like stacking of adjacent liquid layers), such as Al droplets on Al_2O_3, have shown significant supercooling[5,8], underlining the importance of investigating the structure, both parallel and perpendicular to the interface, of these interfacial liquid layers. Indeed, the influence of a solid–liquid interface on the five-fold order inside the liquid has been discussed[25,26]. In the present system, we have thus paid particular attention to the structure of the Au-induced (6×6) reconstruction of the Si(111) surface and its influence on the in-plane structure of the adjacent liquid, revealing a clear link between the structure of this reconstruction and that of the liquid.

Figure 3d shows high resolution measurements of the scattered intensity performed along a symmetry direction of the Si(111) surface, hence crossing its reconstruction peaks. The first and second orders of the liquid structure factor $S(Q)$ both reveal a marked correlation between the appearance of the (6×6) reconstruction peaks and an increase in intensity in the maxima of $S(Q)$. In addition, the radial intensity distribution obtained by integration of all diffraction peaks measured from the (6×6) reconstruction and their subsequent convolution by fast Fourier transform (detailed in Supplementary Fig. 6) compares well to the experimental and theoretical structure factors of the liquid (Fig. 3a), indicating close similarities of the main interatomic distances in the liquid and in the (6×6) structure. Note that our measurements average over a macroscopic surface composed of the free (6×6)Au reconstructed Si(111) surface between islands, and of the interface between the substrate and the islands; the latter covers only a few per cent of the total area. It is thus not strictly possible to conclude the existence of a long-range ordered (6×6) reconstruction at the substrate–droplet interface. However, the evidence of enhanced supercooling in the presence of this reconstruction on the one hand, and the high stability of it on the other hand (demonstrated, for example, by its fast recovery by gentle annealing after having been destroyed by ion bombardment) let us believe that the liquid–solid interface is at least locally reconstructed with the pentagonal order of the Au-(6×6) structure.

Zooming in on the first maximum of the liquids' $S(Q)$ (Fig. 2b) proves that under the influence of the (6×6) reconstruction, the liquid becomes anisotropic: the scattered intensity is more pronounced in the vicinity of the most intense peaks of the (6×6) reconstruction, indicating a structural similarity of the (6×6) structure and the adjacent liquid layers at the local scale. This is further evidenced in Fig. 2c, where scans across the first maximum of $S(Q)$ are presented for different out of plane momentum transfer, Q_z. For large Q_z, the isotropic liquid scattering is separated from a rod of scattering present for all Q_z at a constant in plane momentum transfer ($Q_{||}$) value. This rod is a signature of a lateral ordering in the liquid close to the solid surface. To interpret this correlation between the internal structure of the liquid and that of the (6×6) reconstruction, together with the enhanced supercooling, one needs to compare the theoretical and experimental structure of the liquid with the atomic arrangement of the (6×6) structure.

The detailed atomic structure of the Si(111)-(6×6)Au reconstruction was determined by measuring quantitatively 983 in-plane Bragg superstructure reflections, integrated and corrected for monitor, area, Lorentz and polarization corrections. The in-plane diffraction diagram (Supplementary Fig. 5) has *p6mm* symmetry, resulting in 234 non-equivalent reflections with a 4.5% systematic uncertainty. The data were quantitatively analysed using ROD[27] software for surface structure analysis. Scans perpendicular to the surface on several reconstruction rods showed that this (6×6) superstructure is of monoatomic thickness. The final model ($\chi^2 = 2.8$ with only the Au atoms taken into account) is remarkably close to the model proposed in ref. 20 for the (6×6) surface reconstruction induced by a one-monolayer Au deposit. The atomic structure consists of a fairly disordered surface unit of low (*p31m*) symmetry, incoherently scattering with its twin with respect to the $[1\bar{1}0]$ mirror. It contains several deformed pentagons surrounding the three-fold axes (Fig. 4). The nearest-neighbour distance in these pentagons is 2.86 Å at room temperature, denser than for gold in its bulk f.c.c. structure (2.90 Å at 550 K), but close to the interatomic distance (2.84 Å) in icosahedral Au clusters in the supercooled liquid,

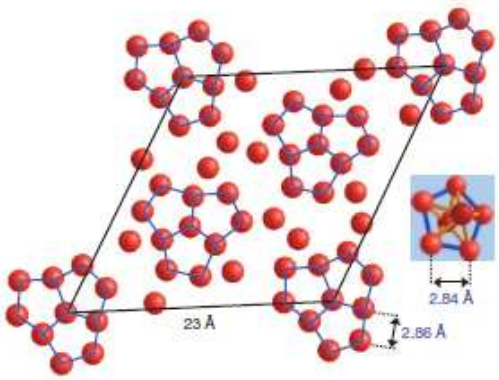

Figure 4 | Au-induced Si(111)-(6 × 6) surface leading to enhanced supercooling. Unit cell (black lozenge) of the complex (6 × 6) reconstruction (only the Au atoms are shown) formed at $T < 673$ K after annealing temperatures $T > 673$ K. A pentagonal cluster (see inset three-dimensional structure) present in the simulated liquid has similar topology and bond length (2.84 Å) as the surface structure (2.86 Å), smaller than in the Au f.c.c. lattice (2.90 Å). Out of 45 atoms in the unit cell, 30 are in a pentagonal environment (interconnected by blue lines).

as deduced from the MDS (Fig. 4 inset). Thus, the (6 × 6) surface structure offers perfect sites to stabilize the five-fold clusters, which in turn stabilize the supercooled metal.

This much enhanced degree of supercooling of liquid AuSi on the Si(111)-(6 × 6) surface compared to other Si surface structures shows the marked influence of a dense pentagonal atomic arrangement at the solid–liquid interface on the short range order and the metastability of a liquid. Although AuSi can be considered as a liquid with quite unusual properties, pentagonal arrangements have been shown to be favourable in a vast range of liquids[7–11]. More generally, solid–liquid interfaces that favour pentagonal local ordering should lead to deep supercooling, because the origin of the barrier to nucleation of crystallographic phases is the formation of local icosahedral order in the liquid. Such interfaces can significantly affect the liquid in contact with them, thus controlling its stability. This may have important implications—for example, perhaps the containerless techniques required today to obtain supercooling could in the future be replaced by icosahedrally coated solid containers.

METHODS SUMMARY

Sample preparation. After oxide removal, the Si(111) surfaces formed a well-defined Si(111)-(7 × 7) reconstruction. Typically, seven atomic layers of Au were deposited at 300 K (room temperature), forming a 1.6-nm-thick film (Fig. 1, step 1). Owing to the low temperature, the Au film crystalline quality was found to be low, but showed a clear preferential epitaxy with identical directions of the two cubic lattices: $[1\bar{1}0]$Au(111)||$[1\bar{1}0]$Si(111). On heating up to 623 K, which is 13 K below $T_E = 636$ K (Fig. 1, step 2), the Au film de-wets to form crystalline islands with a preferential in-plane epitaxy rotated by 19.2° with respect to the aligned epitaxy (that is, $[1\bar{1}0]$Au(111)||$[\bar{2}\bar{3}1]$Si(111)). *In situ* X-ray peak width analysis, together with *ex situ* high resolution secondary electron microscopy and atomic force microscopy, showed islands of average width 150 nm and average height 25 nm (for the seven-monolayer deposit), which is typical for annealed gold layers of similar thickness[28]

time (durations 30 ps, time step 3 fs), the last two runs being in the supercooled regime. More details are available as Supplementary Information.

Received 13 October 2009; accepted 23 February 2010.

1. Turnbull, D. Kinetics of solidification of supercooled liquid mercury droplets. *J. Chem. Phys.* 20, 411–424 (1952).
2. Frank, F. C. Supercooling of liquids. *Proc. R. Soc. Lond. A* 215, 43–46 (1952).
3. Torquato, S. & Jiao, Y. Dense packings of the Platonic and Archimedean solids. *Nature* 460, 876–879 (2009).
4. Reichert, H. *et al.* Observation of five-fold local symmetry in liquid lead. *Nature* 408, 839–841 (2000).
5. Oh, S. H., Kauffmann, Y., Scheu, C., Kaplan, W. D. & Rühle, M. Ordered liquid aluminum at the interface with sapphire. *Science* 310, 661–663 (2005).
6. Greer, A. L. Liquid metals: supercool order. *Nature Mater.* 5, 13–14 (2006).
7. Wochner, P. *et al.* X-ray cross correlation analysis uncovers hidden local symmetries in disordered matter. *Proc. Natl Acad. Sci. USA* 106, 11511–11514 (2009).
8. Steinhardt, P. J., Nelson, D. R. & Ronchetti, M. Icosahedral bond orientational order in supercooled liquids. *Phys. Rev. Lett.* 47, 1297–1300 (1981).
9. Sheng, H. W., Luo, W. K., Alamgir, F. M., Bai, J. M. & Ma, E. Atomic packing and short-to-medium-range order in metallic glasses. *Nature* 439, 419–425 (2006).
10. Schenk, T., Holland-Moritz, D., Simonet, V., Bellissent, R. & Herlach, D. M. Icosahedral short-range order in deeply undercooled metallic melts. *Phys. Rev. Lett.* 89, 075507 (2002).
11. Jakse, N. & Pasturel, A. Local order of liquid and supercooled zirconium by ab initio molecular dynamics. *Phys. Rev. Lett.* 91, 195501 (2003).
12. Wagner, R. S. & Ellis, W. C. Vapor-liquid-solid mechanism of single crystal growth. *Appl. Phys. Lett.* 4, 89–90 (1964).
13. Hannon, J. B., Kodambaka, S., Ross, F. M. & Tromp, R. M. The influence of the surface migration of gold on the growth of silicon nanowires. *Nature* 440, 69–71 (2006).
14. Kim, B. J. *et al.* Kinetics of individual nucleation events observed in nanoscale vapor-liquid-solid growth. *Science* 322, 1070–1073 (2008).
15. Kodambaka, S., Tersoff, J., Reuter, M. C. & Ross, F. M. Germanium nanowire growth below the eutectic temperature. *Science* 316, 729–732 (2007).
16. Hofmann, S. *et al.* Ledge-flow-controlled catalyst interface dynamics during Si nanowire growth. *Nature Mater.* 7, 372–375 (2008).
17. Sutter, E. & Sutter, P. Phase diagram of nanoscale alloy particles used for vapor-liquid-solid growth of semiconductor nanowires. *Nano Lett.* 8, 411–414 (2008).
18. Adhikari, H., Marshall, A. F., Chidsey, C. E. D. & McIntyre, P. C. Germanium nanowire epitaxy: shape and orientation control. *Nano Lett.* 6, 318–323 (2006).
19. Pinardi, A. L., Leake, S. J., Felici, R. & Robinson, I. K. Formation of an Au-Si eutectic on a clean silicon surface. *Phys. Rev. B* 79, 045416 (2009).
20. Grozea, D. *et al.* Direct methods determination of the Si(111)-(6×6)Au surface structure. *Surf. Sci.* 418, 32–45 (1998).
21. Shpyrko, O. G. *et al.* Surface crystallization in a liquid AuSi alloy. *Science* 313, 77–80 (2006).
22. Chen, H. S. & Turnbull, D. Thermal properties of gold-silicon binary alloy near the eutectic composition. *J. Appl. Phys.* 38, 3646–3650 (1967).
23. Sutter, P. W. & Sutter, E. A. Dispensing and surface-induced crystallization of zeptolitre liquid metal-alloy drops. *Nature Mater.* 6, 363–366 (2007).
24. Honeycutt, J. D. & Andersen, H. C. Molecular-dynamics study of melting and freezing of small Lennard-Jones clusters. *J. Phys. Chem.* 91, 4950–4963 (1987).
25. Spaepen, F. Structural model for solid-liquid interface in monoatomic systems. *Acta Metall.* 23, 729–743 (1975).
26. Heni, M. & Lowen, H. Do liquids exhibit local fivefold symmetry at interfaces? *Phys. Rev. E* 65, 021501 (2002).
27. Vlieg, E. ROD: A program for surface X-ray crystallography. *J. Appl. Crystallogr.* 33, 401–405 (2000).
28. Schubert, L. *et al.* Silicon nanowhiskers grown on 111 > Si substrates by molecular-beam epitaxy. *Appl. Phys. Lett.* 84, 4968–4970 (2004).
29. Kresse, G. & Furthmuller, J. Efficiency of ab-initio total energy calculations for metals and semiconductors using a plane-wave basis set. *Comput. Mater. Sci.* 6, 15–50 (1996).

Supplementary Information is linked to the online version of the paper at www.nature.com/nature.

Acknowledgements We thank J. Villain, G. Bauer, H. Reichert, Y. Bréchet and

overall electronic structure of a compound can be thought of as a hybrid of all of its possible resonance structures, it could be that the dianion-containing resonance structure of Braunschweig and colleagues' borole contributes to the unusual stability of the compound.

There is clearly much more work to be done to explore the chemistry of Braunschweig and colleagues' compound. Perhaps most intriguingly, the borole monoanion might open up new routes for the preparation of other borole derivatives that are otherwise difficult to make. If so, maybe we will finally have a chance to fully investigate the chemistry of this fascinating family of organoboron compounds. ■

Kyoko Nozaki is in the Department of Chemistry and Biotechnology, School of Engineering, University of Tokyo, 7-3-1 Hongo, Bunkyo-ku, 113-8656 Tokyo, Japan.
e-mail: nozaki@chembio.t.u-tokyo.ac.jp

1. de Meijere, A. & Diederich, F. (eds) *Metal-Catalyzed Cross-Coupling Reactions* 2nd edn (Wiley, 2004).
2. Elsch, J. J., Galle, J. E. & Kozima, S. *J. Am. Chem. Soc.* **108**, 379–385 (1986).
3. Wakamiya, A., Mishima, K., Ekawa, K. & Yamaguchi, S. *Chem. Commun.* 579–581 (2008).
4. Braunschweig, H., Chiu, C.-W., Radacki, K. & Kupfer, T. *Angew. Chem. Int. Edn* **49**, 2041–2044 (2010).
5. Parsons, T. D., Silf, J. M. & Schaad, L. H. *J. Am. Chem. Soc.* **89**, 3446–3448 (1967).
6. Blumenthal, A., Bissinger, P. & Schmidbaur, H. *J. Organomet. Chem.* **462**, 107–110 (1993).
7. Imamoto, T. & Hikosaka, T. *J. Org. Chem.* **59**, 6753–6759 (1994).
8. Sagawa, Y., Yamashita, M. & Nozaki, K. *Science* **314**, 113–115 (2006).
9. Sagawa, Y., Suzuki, Y., Yamashita, M. & Nozaki, K. *J. Am. Chem. Soc.* **130**, 16069–16079 (2008).
10. Loginov, D. A., Muratov, D. V. & Kudinov, A. R. *Russ. Chem. Bull.* **57**, 1–7 (2008).
11. So, C.-W., Watanabe, D., Wakamiya, A. & Yamaguchi, S. *Organometallics* **27**, 3496–3501 (2008).
12. Herberich, G. E., Wagner, T. & Marx, H.-W. *J. Organomet. Chem.* **502**, 67–74 (1995).
13. Walton, J. C. *et al. J. Am. Chem. Soc.* **132**, 2350–2358 (2010).

MATERIALS SCIENCE

A cloak of liquidity

A. Lindsay Greer

Droplets of a liquid alloy on a silicon surface can rearrange the surface atoms so that they mimic the short-range ordering of atoms in the alloy. Remarkably, this effect inhibits freezing of the droplets.

Promoting freezing in a liquid is conceptually straightforward — you simply need to add suitable templates. The templates can be either 'seeds' of the crystalline phase that would form from the liquid, or small crystals of another material whose atomic-level surface structure in some way matches that of such seeds.

What is much more difficult to conceive of is a solid surface that inhibits freezing by acting as a template for the liquid. However, on page 1174 of this issue, Schöllli *et al.*[1] describe evidence suggesting that such a template is possible. Their results have wide implications not only for fundamental studies of freezing, but also for the practical control of this phase transition.

When a liquid is cooled, there is a thermodynamically defined temperature — the freezing point, or liquidus temperature — at which it should start to crystallize. But the crystal nucleation that initiates freezing requires a driving force, and occurs only at temperatures below the ideal freezing temperature. The cooling of a liquid to below the ideal freezing temperature, known as supercooling (Fig. 1), is of great interest in diverse areas ranging from the control of microstructure in metallic welds and castings[2] to the inhibition (or promotion) of ice formation necessary for the survival of living systems[3]. Although in some situations it is desirable to nucleate crystals at the highest possible temperature by minimizing supercooling, in others the challenge is to avoid nucleation so that liquids and their freezing processes can be studied at the lowest temperature possible (greatest possible supercooling).

Schöllli *et al.*[1] studied the freezing of a liquid gold–silicon alloy near its eutectic (lowest freezing point) composition. Not only is this alloy a useful model system, but it also has practical significance — it is used in the vapour–liquid–solid process for growing silicon nanowires[4]. The authors formed microscopic islands of gold on a single-crystal silicon substrate and heated them until they melted, whereupon some of the silicon dissolved into the gold to form liquid-alloy droplets. On cooling, these droplets froze at a temperature that was reproducible over repeated heating–cooling cycles, but that depended greatly on the upper temperature limit of the heating.

Using an X-ray scattering technique under ultra-high vacuum conditions, Schöllli *et al.*[1] characterized the structure of the liquid–substrate interfaces in their system *in situ*. They found that on crystallographically defined silicon substrates (for which particular planes within the lattice were exposed at the surface) the freezing point of the gold–silicon alloy was generally 563 kelvin. By performing a detailed analysis of extensive X-ray data acquired at a wide range of angles to the substrate, the authors showed that this freezing point corresponds to a slight, gold-induced reconstruction of the atomic arrangement of the silicon surface. But when the team had previously heated the liquid to temperatures above 673 K, the onset of freezing was remarkably depressed to 513 K. In this case, the authors observed that the silicon had undergone a more radical reconstruction to yield what is known as a 6×6 superstructure.

PHOTOLIBRARY.COM

Figure 1 | Natural supercooling. These trees are covered in rime ice, which forms when supercooled water droplets in the atmosphere come into contact with cold objects and freeze rapidly.

The freezing point of the alloy in contact with the 6×6 silicon surface is about 120 K below that of eutectic gold–silicon, but Schöllli *et al.* point out that the eutectic freezing temperature is not the most appropriate reference point from which supercooling of the system should be measured. As the liquid alloy droplets cool, silicon comes out of solution and redeposits on the substrate, enriching the droplets in gold. The observed freezing point of 513 K therefore represents a supercooling of about 360 K below the liquidus of the resulting composition. This is more than 40% of the expected freezing temperature, an exceptionally high value for a metallic system[5].

This supercooling is all the more

NATURE|Vol 464|22 April 2010

remarkable because of the ordering of the liquid at the solid–liquid interface. It is accepted that a liquid in contact with a planar solid shows out-of-plane ordering — the liquid atoms form layers parallel to the surface of the solid[6]. This might be thought to favour crystallization of the liquid, but whether or not this is so depends on the nature of the atomic ordering within each layer (in-plane ordering), the characterization of which has proved challenging[7]. In-plane ordering is exactly what would be expected when a liquid comes into contact with a substrate that acts as a template for crystal nucleation in freezing.

Schöll *et al.*[1] have succeeded in the difficult task of characterizing in-plane order in the liquid gold–silicon alloy adjacent to the 6 × 6 silicon surface. They found that the liquid is anisotropic, with atomic positions strongly correlated with the structure on the underlying surface. It is remarkable that this correlation with a periodic surface pattern impedes the crystallization of the liquid, rather than inducing it.

The researchers[1] also characterized the structure of the gold–silicon liquid away from the silicon substrate and found that, in common with most metallic liquids[8], it shows icosahedral short-range order that becomes more pronounced on cooling. Crucially, the authors observed that the pentagonal clusters of atoms typical of the icosahedral order seem to be stabilized by similar pentagonal arrangements in the 6 × 6 silicon superstructure (see Fig. 4 on page 1177). However, when the alloy droplets freeze on the 6 × 6 silicon surface, the resulting gold crystals form in random orientations. This suggests that the substrate has no orienting role in freezing; the actual site and mechanism of crystal nucleation remain undetermined.

For several years, there has been intense interest in attaining a large supercooling effect of liquids before the onset of freezing. To avoid crystal nucleation caused by contact with a solid, the favoured strategy is to process the liquid without using a container. This can be done in various ways[9], including by levitating liquid drops electromagnetically, electrostatically or acoustically, or by studying drops as they fall through a tube or tower. Because the surface energies of most liquids are lower than those of the crystals that form from them[10], free surfaces — in these experiments, the liquid surfaces at air–liquid interfaces — also stabilize the liquid state of levitating or free-falling drops. The work of Schöll *et al.*[1], however, opens up an attractive alternative to dispensing with the container: why not just disguise the container's surface as a liquid? ■

A. Lindsay Greer is in the Department of Materials Science and Metallurgy, University of Cambridge, Cambridge CB2 3QZ, UK.
e-mail: alg13@cam.ac.uk

1. Schöll, T. U. et al. *Nature* **464**, 1174–1177 (2010).
2. Spittle, J. A. *Int. Mater. Rev.* **51**, 247–269 (2006).
3. Zachariassen, K. E. & Kristiansen, E. *Cryobiology* **41**, 257–279 (2000).
4. Hannon, J. B., Kodambaka, S., Ross, F. M. & Tromp, R. M. *Nature* **440**, 69–71 (2006).
5. Kelton, K. F. *Solid State Phys.* **45**, 75–177 (1991).
6. Oh, S. H., Kauffmann, Y., Scheu, C., Kaplan, W. D. & Rühle, M. *Science* **310**, 661–663 (2005).
7. Greer, A. L. *Nature Mater.* **5**, 13–14 (2006).
8. Lee, G. W. et al. *Phys. Rev. B* **77**, 184102 (2008).
9. Herlach, D. M., Cochrane, R. F., Egry, I., Fecht, H. J. & Greer, A. L. *Int. Mater. Rev.* **38**, 273–347 (1993).
10. Oxtoby, D. W. *Nature* **347**, 725–730 (1990).

INFECTIOUS DISEASE

Listeria does it again

Julian I. Rood

Proteins are synthesized by ribosomes, and then commonly undergo further modifications. A new example of how these host-cell processes can be subverted by a pathogenic bacterium has come to light.

There are many ways by which pathogenic bacteria produce the cell and tissue damage that leads to human disease. On page 1192 of this issue Ribet *et al.*[1] reveal another such mechanism — they show that *Listeria monocytogenes* can alter an essential host-cell biochemical pathway, and potentially decrease the ability of the host to respond to infection.

The development of an infectious disease is a tactical war between the attacking armaments of the invading pathogen and the defence mechanisms of the host. With some pathogens a single potent virulence factor will suffice. With others the host cell has to counter many different factors, as is the case when the cell is attacked by *L. monocytogenes*. This food-borne bacterium can cause several diseases, including gastroenteritis, septicaemia and meningitis, and also miscarriage[2]. It produces several virulence factors that enable it to invade host cells, and to grow and multiply within them. The complexity of this process makes it a model bacterial pathogen for understanding the infectious-disease process, from both a host and a pathogen perspective. Examples of discoveries stemming from the study of *L. monocytogenes* (Fig. 1) include the determination of the role of extracellular toxins in bacterial escape from the phagolysosome (the bactericidal vacuole of the invaded host cell),

50 & 100 YEARS AGO

50 YEARS AGO

This article describes a model which imitates certain aspects of morphogenesis and maintenance in a developing embryo. The model consists of a number of artificial 'cells' (constructed from radio parts) which can stimulate and inhibit one another by means of connexions which are made through a switchboard. The pattern of activity generated, representing the growth pattern, was found to bear a remarkable resemblance to certain aspects of morphogenesis ... Many other properties of our system, with larger numbers of cells and with other ways of connecting them together, are reminiscent of the properties of growing embryos: for example, the patterns are in general homeostated — a disturbance producing only a temporary change in the pattern. Discrete differences (such as 'on' or 'off') appear between neighbouring cells, in contrast to the continuous differences which would be expected on a purely humoural mechanism of growth control.

Dr. R. J. Goldacre and A. D. Bean
From *Nature* 23 April 1960.

100 YEARS AGO

In her letter to NATURE on March 24 Miss I. Sollas remarks on the "canary-yellow" colour "in members of the stoat family when the winter whitening is incomplete," adding, "there can thus be little doubt that the yellow body produced artificially in the fur of the albino rat is a substance similar to the yellow pigment of the stoat's winter coat ..." I do not know whether it has been recorded ... that a stoat's fur of the purest white will, after exposure to light in a museum case for a time, varying with the intensity of the light, invariably turn distinctly yellow — tainter, however, than "canary-yellow." ... The usual reason assigned for the change is the absorption by the hairs of a small amount of fat out of the skin, induced by the light and heat of summer.

Henry O. Forbes
From *Nature* 21 April 1910.

V : Nouvelles publications depuis le rapport d'audit

-"*Substrate-enhanced supercooling in AuSi eutectic droplets*"
T.U. Schülli, R. Daudin, G. Renaud, A. Vaysset, O. Geaymond and A. Pasturel,
Nature **464**, 1174 (2010).

- "*Confinement induced phase transition in a DNA-lipid hydrated complex*"
E. Andreoli de Oliveira , E. R. Teixeira da Silva, A. Fevrier, E. Grelet, F. Nallet and L. Navailles
Europhysics Letters **91** (2010) 28001

- "*Dislocation storage in single slip-oriented Cu micro-tensile samples: New insights via X-ray microdiffraction*"
C. Kirchlechner; D. Kiener; C. Motz; S. Labat; N. Vaxelaire; O. Perroud; J. -S. Micha; O. Ulrich; O. Thomas; G. Dehm; J. Keckes
Philosophical Magazine (2010) **1478**- 6443

-"*Elastic strain relaxation in GaN/AlN nanowire superlattice*"
O. Landré, D. Camacho, C. Bougerol; Y.M. Niquet, V. Favre-Nicolin, G. Renaud, H. Renevier and B. Daudin,
Phys. Rev. B **81**, 153306 (2010).

-"*Probing nanoscale structural and order/disorder phase transitions of supported Co-Pt clusters under annealing*"
P.Andreazza, C. Mottet, C. Andreazza-Vignolle, J. Penuelas, H. C. N. Tolentino, M. De Santis, R. Felici, and N. Bouet
Phys. Rev. B **82**, 155453 (2010)

-"*Study of the formation, evolution and dissolution of interfacial defects in silicon wafer bonding*,"
S. Vincent, J. D. Penot, I. Radu, F. Letertre, and F. Rieutord,
J. Appl. Phys., **107**, 093513, 2010.

- "*Supported bilayers: Combined specular and diffuse X-ray scattering*"
Malaquin L, Charitat T, Daillant J
Euro. Phys. J. **E 31** (2010) 285

- "*Hydrated cholesterol: Phospholipid domains probed by synchrotron radiation*"
Solomonov I, Daillant J, Fragneto G, Kjaer K, Micha J.S., Rieutord F, Leiserowitz L
Euro. Phys. J. **E 30** (2009) 215

-"Nanoscale Patterning by C60 Ordering on Pt(110)"
Torrelles X, Langlais V, De Santis M, Tolentino HCN et al.
J. Phys. Chem. C **114,** 15645 (2010)

- "*Influence of the U_3O_7 domain structure on cracking during the oxidation of UO_2*"
Desgranges, L; Palancher, H; Gamaleri, M, Micha J.S., Optasanu V, Raceanu L, Montesin T, Creton N.
J. Nucl. Mat. **402** (2010) 167

- "*Determination of global and local residual stresses in SOFC by X-ray diffraction*"
Villanova J, Sicardy O, Fortunier R, Micha J.S., Bleuet P
Nucl. Inst. Meth. Phys. **B 268** (2010) 282

- "*X-ray microbeam strain investigation on Cu-MEMS structures*"
Perroud O, Vayrette R, Rivero C, Thomas O, Micha J.S., Ulrich O
Microelectronic Engineering **87** (2010) 394

-"*Defect formation at hydrophilic silicon bonding interfaces*,"
F. Rieutord, S. Vincent, J. D. Penot, H. Moriceau, and I. Radu,
ECS Transactions, **33**, 451, 2010.

- "*Efficiency of H2O diffusion barriers at Si-Si direct bonding interfaces*,"
H. Moriceau, F. Rieutord, L. Libralesso, C. Ventosa, F. Fournel, C. Morales, T. Mc Cormick, T. Chevolleau, and I. Radu,
ECS Transactions, **33**, 467, 2010.

- "*An overview of patterned metal/dielectric surface bonding: mechanism, alignment and characterization*,"
L. Di Cioccio, P. GUEGUEN, R. Taibi, D. Landru, G. Gaudin, C. Chappaz, F. Rieutord, F. de Crecy, I. Radu, L.-L. Chapelon, and L. Clavelier,
ECS Transactions, **33**, 3, 2010.

-"*Single Crystal Silicon Film Transfer onto polymer*,"
M. Argoud, H. Moriceau, C. Fretigny, F. Rieutord, C. Morales, and L. Clavelier,
ECS Transactions, **33**, p217, 2010.

Submitted:

- "*Twins and their boundaries during homoepitaxy on Ir(111)*"
S. Bleikamp, J. Coraux, O. Robach, G. Renaud and T. Michely,
Phys. Rev. B (submitted).

-"*In-depth atomic structure and composition of the 2×N reconstruction of the initial growth stages of the Ge wetting layer on Si(001) by surface x-ray diffraction*",
T. Zhou, G. Renaud, J. Issartel, C. Revenant, T.U. Schülli, R. Felici and A. Malachias,
Phys. Rev. B (submitted).

-Highly anisotropic epitaxial L10 FePt on Pt(001)
Márcio M. Soares, Hélio C.N. Tolentino, Maurizio De Santis, Aline Y. Ramos, and Júlio C. Cezar
submitted to Journal of Applied Physics 2010

-"*A new white beam X-ray micro-diffraction setup on the BM32 beamline at ESRF,"*
O. Ulrich, X. Biquard, P. Bleuet, O. Geaymond, P. Gergaud, J. S. MICHA, O. Robach, and F. Rieutord,
Review of Scientific Instruments, submitted, 2010.

-"*A combined in situ GISAXS and GIXD study of the growth of Ge islands on pit-patterned Si(001) substrates*."
M.-I. Richard, T.-U. Schülli, G. Renaud, Z;-Z. Zong and G. Bauer,
Applied Surf. Sci. (2010)

-"*In situ composition and strain of Ge islands on Si(001) during growth by grazing-incidence multiwavelength anomalous diffraction*".
M.-I. Richard, T. U. Schülli, G. Renaud, V. Favre-Nicolin; G. Bauer
PRL, submitted